

1 **Inflammasome-mediated antagonism of type I interferon enhances *Rickettsia* pathogenesis**

2

3 Thomas P. Burke^{1*}, Patrik Engström¹, Roberto A. Chavez^{1,2}, Joshua A. Fonbuena¹, Russell E. Vance^{1,2},

4 Matthew D. Welch^{1,3*}

5

6 ¹Department of Molecular and Cell Biology, University of California, Berkeley, Berkeley, CA, 94720 USA

7 ²Howard Hughes Medical Institute

8 ³Lead contact

9 *Correspondence: tburke@berkeley.edu (T.P.B), welch@berkeley.edu (M.D.W.)

10 **Summary**

11 Inflammasomes and interferons constitute two critical arms of innate immunity. Most facultative bacterial
12 pathogens that inhabit the host cell cytosol avoid activating inflammasomes and are often resistant to
13 killing by type I interferon (IFN-I). We report that the human pathogen *Rickettsia parkeri*, an obligate
14 intracellular pathogen that resides in the cytosol, is sensitive to IFN-I. The mechanism of IFN-I-
15 dependent restriction requires the transcription factor IRF5, which upregulates anti-rickettsial factors
16 including guanylate-binding proteins and iNOS. However, *R. parkeri* curtails cGAS-dependent IFN-I
17 production by causing caspase-11-dependent pyroptosis. *In vivo*, inflammasome activation antagonizes
18 IFN-I production, enhancing *R. parkeri* abundance in the spleen. Mice lacking either IFN-I or IFN- γ
19 signaling are resistant to infection, but mice lacking both rapidly succumb, revealing that both interferons
20 are required to control *R. parkeri*. This study illuminates how an obligate cytosolic pathogen exploits the
21 intrinsic trade-off between cell death and cytokine production to escape killing by innate immunity.

22

23 **Highlights**

- 24 • *Rickettsia* killed by GBPs activates caspase-11 and GSDMD, promoting pyroptosis
- 25 • *Rickettsia* exploits pyroptosis to avoid cGAS-dependent type I interferon
- 26 • IRF5, GBPs, and iNOS contribute to controlling *R. parkeri* infection
- 27 • *Ifnar*^{-/-}*Ifngr*^{-/-} mice succumb to infection, uncovering a mouse model to study *R. parkeri*

28

29 **Keywords**

30 Inflammasome; type I interferon; IFN- γ ; *Rickettsia parkeri*; IRF5; guanylate-binding proteins; GBP2;
31 GBP5; caspase-11; cGAS

32

33

34

35

36

37 **Introduction**

38 The innate immune response to microbial pathogens depends on upregulation of antimicrobial
39 factors, secretion of cytokines, and activation of host cell death pathways (Jorgensen and Miao, 2015;
40 Meunier and Broz, 2016; Mitchell and Isberg, 2017; Randow et al., 2013). Innate immune responses
41 have been characterized during infection with facultative intracellular bacterial pathogens such as
42 *Listeria monocytogenes* and virulent *Francisella* species, as well as viruses, which inhabit the host cell
43 cytosol (Brubaker et al., 2015; McNab et al., 2015; Wallet et al., 2016). However, less well understood
44 are the innate immune responses to obligate intracellular bacterial pathogens. Spotted fever group
45 (SFG) *Rickettsia* spp. are tick-borne pathogens that cause spotted fever diseases worldwide (Walker
46 and Ismail, 2008). As obligate intracellular bacteria that replicate exclusively in the host cell cytosol,
47 SFG *Rickettsia* spp. must continually interface with host innate immune sensors. Therefore, they
48 presumably have evolved sophisticated mechanisms to avoid or even exploit innate immune responses.

49 Following infection and subsequent detection of pathogen associated molecular patterns
50 (PAMPS) by host cell sensors (Takeuchi and Akira, 2010), cytokines including type I interferon (IFN-I)
51 are upregulated. For example, the detection of cytosolic DNA by cyclic GMP-AMP synthase (cGAS)
52 results in activation of the downstream adaptor stimulator of IFN genes (STING) and transcription
53 factors including IFN regulatory factor 3 (IRF3) to upregulate IFN-I expression and secretion (Sun et al.,
54 2013). Binding of IFN-I to the interferon- α/β receptor (IFNAR) then activates a signaling cascade that
55 upregulates the expression of hundreds of interferon-stimulated genes (ISGs), mobilizing the cytosol to
56 an antimicrobial state (MacMicking, 2012; Meunier and Broz, 2016).

57 Previous studies revealed that *L. monocytogenes* is resistant to the killing effects of IFN-I in
58 macrophages (Reutterer et al., 2008; Woodward et al., 2010), and in fact, this pathogen actively
59 secretes STING agonists that stimulate IFN-I production (Burdette et al., 2011; Woodward et al., 2010).
60 IFN-I enhances *L. monocytogenes* as well as *Francisella novicida* pathogenicity *in vivo* (Auerbuch et
61 al., 2004; Carrero, 2013; Henry et al., 2010; O'Connell et al., 2004; Storek et al., 2015), demonstrating
62 that these bacterial pathogens benefit from IFN-I signaling. In contrast, IFN-I has a critical role in
63 restricting viral replication, and therefore the effects of IFN-I signaling on pathogens that inhabit the

64 cytosol are often regarded as anti-viral but not anti-bacterial (Boxx and Cheng, 2016; McNab et al.,
65 2015; Stetson and Medzhitov, 2006).

66 Cytosolic PAMPs can also be recognized by inflammasomes, resulting in host cell death. For
67 example, sensing of PAMPs such as microbial DNA by nucleotide-binding domain and leucine-rich
68 repeat containing gene family (NLR) proteins causes their oligomerization and subsequent activation of
69 the protease caspase-1 (Lamkanfi and Dixit, 2014; Strowig et al., 2012). Similarly, direct binding of
70 bacterial lipopolysaccharide (LPS) to the non-canonical inflammasome caspase-11 causes its
71 oligomerization and activation (Aachoui et al., 2013; Hagar et al., 2013; Kayagaki et al., 2013; Shi et
72 al., 2014). Active caspases-1 and -11 cleave the pore-forming protein gasdermin D (GSDMD),
73 promoting pyroptosis, a rapid lytic host cell death (Kayagaki et al., 2015; Shi et al., 2015). Pyroptosis
74 curtails microbial replication and exposes microbes to the extracellular environment where they can be
75 targeted by immune factors such as phagocytes and antibodies. To avoid inflammasome activation, *F.*
76 *novicida* modifies its LPS, enabling it to avoid caspase-11 (Hagar et al., 2013; Wallet et al., 2016).
77 Additionally, *L. monocytogenes* and *F. novicida* minimize bacteriolysis to prevent the release of DNA
78 (Peng et al., 2011; Sauer et al., 2010), and *L. monocytogenes* downregulates expression of flagellin (an
79 activator of the inflammasome) during infection (Shen and Higgins, 2006). These virulence strategies
80 reveal that pathogens can benefit from circumventing inflammasome activation. Interestingly,
81 inflammasome activation antagonizes IFN-I production (Banerjee et al., 2018; Corrales et al., 2016;
82 Jabir et al., 2014; Liu et al., 2018), and IFN-I can antagonize inflammasome activation (Guarda et al.,
83 2011; Inoue et al., 2012). This suggests that the immune system may flip a switch between cell-intrinsic
84 anti-viral and anti-bacterial responses.

85 Despite these advances, the role for IFN-I, inflammasomes, and other innate immune responses
86 during infection by obligate intracellular bacteria is not fully understood. IFN-I has modest anti-rickettsial
87 effects in immortalized endothelial cells *in vitro* (Colonne et al., 2011; 2013; Turco and Winkler, 1990).
88 In regards to the inflammasome, caspase-1 is required for the production of IL-1 β during *R. australis*
89 infection (Smalley et al., 2016). Many studies have also established a critical role for interferon- γ (IFN-
90 γ) and nitric oxide as anti-rickettsial factors (Feng et al., 1994; Li et al., 1987; Turco and Winkler, 1993;

91 Turco et al., 1998; Walker et al., 1997). However, the role for pyroptosis, IFN-I, and their relationships
92 to IFN- γ during *Rickettsia* infection remain unknown. Since *Rickettsia* obligately reside within the host
93 cytosol, we hypothesize that they have evolved sophisticated and distinctive measures to manipulate
94 the inflammasome and IFN-I response to their benefit.

95 Here, we investigated the roles for host cell death, IFN-I signaling, and antimicrobial factors in
96 controlling *R. parkeri* infection at the molecular, cellular, tissue, and organismal levels. We observed
97 that, unlike facultative cytosolic bacterial pathogens, *R. parkeri* intracellular growth is restricted by IFN-
98 I in macrophages *in vitro*. If *R. parkeri* is killed in the host cytosol by guanylate-binding proteins (GBPs),
99 the inflammasome is activated, thus curtailing IFN-I production. Consistently, we discovered that *R.*
100 *parkeri* antagonized IFN-I production *in vivo* via inflammasome activation, which has tissue-specific
101 effects on controlling bacterial replication. We also found that both IFN-I and IFN- γ are critical for
102 controlling *R. parkeri* infection in mice, and propose that mice lacking interferon signaling can serve as
103 a robust animal model for investigating *Rickettsia* pathogenesis. Our data suggest an unprecedented
104 strategy whereby a bacterial pathogen exploits the inherent antagonism between the inflammasome
105 and IFN-I response to promote its pathogenesis.

106

107 **Results**

108 **Inflammasome activation promotes *R. parkeri* growth in macrophages by antagonizing the IFN- 109 I response**

110 Although previous studies have investigated the roles of IFN-I and inflammasomes during
111 infection by facultative intracellular pathogens, little is known for obligate intracellular pathogens
112 including *R. parkeri*. Previous reports suggested that IFN-I causes a ~50% reduction in *Rickettsia* spp.
113 growth in immortalized endothelial cells (Colonne et al., 2011; 2013; Turco and Winkler, 1990). *In vivo*,
114 both endothelial cells (Feng et al., 1993; Sahni and Rydkina, 2009) and other cell types including
115 macrophages (Banajee et al., 2015; Feng et al., 1993; Osterloh et al., 2016; Papp et al., 2016; Walker
116 et al., 1999) are targeted by *Rickettsia* spp. during infection. However, the effect of IFN-I on *Rickettsia*
117 spp. replication in primary macrophages was unknown. We infected wild type (WT) primary bone

118 marrow-derived macrophages (BMDMs) with *R. parkeri* or *L. monocytogenes*, treated them with
119 recombinant IFN- β , and measured the impact on bacterial growth (by counting plaque-forming units
120 (PFU) for *R. parkeri* or colony-forming units (CFU) for *L. monocytogenes*). IFN- β caused a dose-
121 dependent restriction of *R. parkeri* growth (**Figure 1A**), whereas it had no effect on *L. monocytogenes*
122 (**Figure 1B**). We further assessed whether each of these pathogens elicited an IFN-I response during
123 infection by testing supernatants from infected BMDMs for their ability to stimulate expression of an
124 IFN-responsive luciferase reporter. *R. parkeri* infection did not induce appreciable IFN-I expression,
125 whereas *L. monocytogenes* elicited a robust response (**Figure 1C**). These data suggest that, although
126 *R. parkeri* is sensitive to IFN-I, it elicits low amounts of IFN-I and therefore grows robustly in
127 macrophages.

128 We next investigated how *R. parkeri* escapes inducing IFN-I by examining the interaction
129 between *R. parkeri* and the inflammasome, leveraging the ability to generate BMDMs from mice
130 genetically deficient in inflammasome components. First, we focused on caspase-1, apoptosis-
131 associated speck-like protein containing CARD (ASC), and the non-canonical inflammasome
132 component caspase-11. WT and mutant BMDMs were infected with *R. parkeri* and bacterial-induced
133 cell death, a readout of inflammasome-dependent pyroptosis, was monitored at 24 h post infection (hpi)
134 using a lactate dehydrogenase (LDH) release assay. Infected *Casp1*^{-/-} and *Asc*^{-/-} mutant BMDMs
135 exhibited ~40% death, similar to WT cells (**Figure 1D**). In contrast, cell death was significantly reduced
136 in *Casp11*^{-/-} mutant BMDMs, and little cell death was observed in *Casp1*^{-/-}*Casp11*^{-/-} double mutant
137 BMDMs (**Figure 1D**). Because caspases-1 and -11 activate pyroptosis by cleaving the pore-forming
138 protein GSDMD, we next measured host cell death in *Gsdmd*^{-/-} BMDMs. Compared to *Casp1*^{-/-} or
139 *Casp11*^{-/-} single mutants, *Gsdmd*^{-/-} BMDM cell death was reduced, but it was not abolished as in the
140 *Casp1*^{-/-}*Casp11*^{-/-} double mutant cells (**Figure 1D**). These data reveal that the majority of *R. parkeri*-
141 induced host cell death in macrophages depends on caspase-11 and GSDMD. To a lesser extent, *R.*
142 *parkeri* activates caspase-1-dependent and GSDMD-independent cell death.

143 As infections proceeded to 96 h, we observed that WT BMDMs became rounded and non-
144 adherent, whereas many *Casp1*^{-/-}*Casp11*^{-/-} double mutant cells remained adherent, similar to uninfected

145 cells (**Figure 1E**). When we measured the number of infectious bacteria in these cells by counting PFU,
146 we observed a reduction in the number of bacteria in *Casp1^{-/-}Casp11^{-/-}* BMDMs, whereas the number
147 of bacteria increased over time in WT BMDMs (**Figure 1F**). There was also a reduction of infectious
148 bacteria in *Casp11^{-/-}* and *Gsdmd^{-/-}* single mutant BMDMs, albeit less pronounced than for the *Casp1^{-/-}*
149 *Casp11^{-/-}* double mutants (**Figure 1F**). Thus, a subpopulation of *R. parkeri* appears to exploit activation
150 of caspase-11 and GSDMD to promote replication of the remaining population.

151 Cytokines including IFN-I and TNF- α are produced by macrophages and can exert antimicrobial
152 activity (Carrero, 2013; Weiss and Schaible, 2015). In addition, IFN-I is overproduced in cells lacking
153 the inflammasome (Corrales et al., 2016; Liu et al., 2018). Hence, we hypothesized that *R. parkeri*-
154 infected *Casp1^{-/-}Casp11^{-/-}* BMDMs were secreting increased levels of IFN-I that restricted *R. parkeri*
155 growth. We therefore tested the bactericidal effects of adding supernatants from infected *Casp1^{-/-}*
156 *Casp11^{-/-}* cells to WT BMDMs that were infected with *R. parkeri*. We found that this supernatant
157 restricted bacterial growth in a dose-dependent manner (**Figure 1G**). Furthermore, IFN-I secretion was
158 increased at least 15-fold in infected *Casp1^{-/-}Casp11^{-/-}* double mutant and *Casp11^{-/-}* and *Gsdmd^{-/-}* single
159 mutant cells (**Figure 1H**). To test whether IFN-I secreted from infected *Casp1^{-/-}Casp11^{-/-}* BMDMs was
160 necessary for bacterial killing, we transferred the supernatant from infected *Casp1^{-/-}Casp11^{-/-}* to infected
161 *Ifnar^{-/-}* BMDMs, which lack the IFN-I receptor and hence are not responsive to IFN-I. The supernatant
162 had no effect on bacteria growth in *Ifnar^{-/-}* cells (**Figure 1G**). Supernatants from infected *Casp1^{-/-}Casp11^{-/-}*
163 ^{-/-} cells were also treated with an anti-IFNAR antibody to prevent IFN-I signaling, and this similarly
164 restored bacterial growth (**Figure 1I**). To further test whether IFN-I was the inhibitory factor, we bred
165 mice lacking *Ifnar*, *Casp1*, and *Casp11* (*Casp1^{-/-}Casp11^{-/-}Ifnar^{-/-}*), infected BMDMs from these mice, and
166 observed that growth of *R. parkeri* was restored (**Figure 1I**). A similar series of experiments failed to
167 show a role for TNF- α in killing *R. parkeri* (**Figure S1**). Together, these findings demonstrate that
168 activation of the inflammasome allows *R. parkeri* to avoid killing by IFN-I.

169

170 **Pyroptosis masks cGAS-induced IFN-I**

171 It remained unclear whether activation of host immune sensors was due to release of *R. parkeri*
172 ligands such as LPS or DNA. We therefore sought to identify the host sensor required for the increased
173 IFN-I production observed in infected *Casp1^{-/-}Casp11^{-/-}* cells. We bred *Cgas^{-/-}*, *Sting^{gt/gt}*, and *Tlr4^{-/-}* to
174 *Casp1^{-/-}Casp11^{-/-}* mice to generate triple mutants (*Casp1^{-/-}Casp11^{-/-}Cgas^{-/-}*, *Casp1^{-/-}Casp11^{-/-}Sting^{gt/gt}*,
175 and *Casp1^{-/-}Casp11^{-/-}Tlr4^{-/-}*) and then infected BMDMs from these mice. As expected, due to their
176 inability to induce pyroptosis, all three triple mutants exhibited reduced host cell death, similar to levels
177 seen for *Casp1^{-/-}Casp11^{-/-}* double mutants (**Figure 2A**). We next measured IFN-I secretion and found
178 that infected *Casp1^{-/-}Casp11^{-/-}Tlr4^{-/-}* cells maintained increased levels of IFN-I, similar to *Casp1^{-/-}*
179 *Casp11^{-/-}* cells (**Figure 2B**). In contrast, *Casp1^{-/-}Casp11^{-/-}Cgas^{-/-}* and *Casp1^{-/-}Casp11^{-/-}Sting^{gt/gt}*
180 macrophages exhibited reduced IFN-I secretion, below levels of infected WT cells (**Figure 2B**). To
181 determine whether the amount of IFN-I production correlated with an effect on bacterial growth, we also
182 measured PFU over time. Mutation of *Cgas* or *Sting* in the *Casp1^{-/-}Casp11^{-/-}* background rescued growth
183 of *R. parkeri* (**Figure 2C**) (for unknown reasons at 96 hpi, bacterial burdens were consistently lower in
184 *Casp1^{-/-}Casp11^{-/-}Cgas^{-/-}* and *Casp1^{-/-}Casp11^{-/-}Sting^{gt/gt}* cells than in WT cells). In contrast, mutation of
185 *Tlr4* in the *Casp1^{-/-}Casp11^{-/-}* background did not rescue bacterial growth. Together, these data in
186 macrophages demonstrate that caspase-11 activation masks cGAS-dependent IFN-I production, and
187 are consistent with the notion that pyroptosis prevents IFN-I production (Corrales et al., 2016; Liu et al.,
188 2018). This observation suggests that, in cells where bacteria release DNA to activate cGAS, they also
189 release LPS to activate caspase-11.

190

191 **IRF5-regulates antimicrobial genes and is required for IFN-I-dependent killing of *R. parkeri***

192 The host factors that restrict *R. parkeri* cytosolic growth downstream of IFN-I are poorly
193 understood, in part because IFN-I upregulates hundreds of ISGs, complicating the ability to identify
194 specific antimicrobial factors. To narrow the list of potential ISGs that restrict *R. parkeri* growth, we first
195 tested whether a specific IRF was required for killing *R. parkeri* upon IFN-I treatment. We analyzed
196 bacterial growth over time following bacterial infection of WT, *Irf1^{-/-}*, *Irf3^{-/-}Irf7^{-/-}*, or *Irf5^{-/-}* mutant BMDMs
197 and treatment with IFN-I. We observed that mutation of *Irf5* significantly rescued bacterial growth

198 compared to WT cells, whereas mutation of *Irf1* or both *Irf3* and *Irf7* caused a modest increase in growth
199 (**Figure 3A**). This suggested that genes specifically regulated by IRF5 restrict *R. parkeri*.

200 To identify genes significantly and specifically regulated by IRF5, we performed high-throughput
201 RNA-sequencing (RNAseq) on the different WT, *Irf1*^{-/-}, *Irf3*^{-/-}*Irf7*^{-/-}, or *Irf5*^{-/-} mutant BMDMs upon infection
202 and IFN-I treatment. To limit the identification of genes not directly responsible for bacterial killing, we
203 isolated RNA at 12 hpi, the earliest time when bacterial killing was observed (**Figure 3B**). Analysis of
204 the RNAseq data revealed that 136 genes were upregulated >4.0-fold in infected IFN-I-treated cells
205 when compared to infected untreated cells (**Table S1**). Among these, 82 were not as highly upregulated
206 (>1.5-fold difference) in infected IFN-I-treated *Irf5*^{-/-} cells when compared to infected IFN-I-treated WT
207 cells, suggesting that many were regulated by IRF5. We then compared the expression of these genes
208 between infected IFN-I-treated *Irf5*^{-/-} and *Irf1*^{-/-} and *Irf3*^{-/-}*Irf7*^{-/-} cells, and 36 had higher expression in *Irf1*^{-/-}
209 and *Irf3*^{-/-}*Irf7*^{-/-} cells than in *Irf5*^{-/-} cells. From the analysis of the RNA-seq data, we conclude that 36
210 genes are significantly and specifically upregulated by IRF5 during *R. parkeri* infection and IFN-I
211 treatment (**Table S1**).

212 Many of the 36 genes encode known anti-viral and anti-bacterial proteins, including *Gbp2*, *Gbp5*,
213 *Rsad2* (encoding Viperin), *Ifit1*, *Ifit2*, *Mx1*, and *Mx2* (**Figure 3C**). The RNA-seq also identified *Nos2*,
214 encoding inducible nitric oxide synthase (iNOS), which is required for controlling *Rickettsia* spp.
215 infection (Feng and Walker, 2000; Turco and Winkler, 1993; Turco et al., 1998; Walker et al., 1997),
216 although its expression was also dependent on IRF1 (**Figure 3C**, right side). Together, these data
217 demonstrate that IRF5 is critical for controlling *R. parkeri* upon IFN-I signaling, perhaps due to
218 upregulating ISGs such as the GBPs and iNOS.

219

220 **GBPs and nitric oxide contribute to restricting *R. parkeri* growth in macrophages**

221 We next assessed whether the IRF5-regulated genes that have previously known antimicrobial
222 activity are important for inhibiting *R. parkeri* growth in the presence or absence of IFN-I. We derived
223 BMDMs from the femurs of mice lacking *Ifit1*, *Ifit2*, *Rsad2*, *LipG* (the gene most highly upregulated by
224 IFN-I), and the chromosome 3 cluster of *Gbps* (*Gbp*^{chr3}) (Yamamoto et al., 2012), which includes *Gbp2*,

225 *Gbp5* and three other *Gbp* genes. Bacterial growth was then measured upon IFN-I treatment. In IFN-I-
226 treated *Gbp^{chr3-/-}* macrophages, bacterial growth was increased 3-to-5-fold compared with that in WT
227 IFN-I-treated macrophages (**Figure 4A**). No change in bacterial growth was observed in the other
228 mutant macrophages upon IFN-I treatment (**Figure S2B**). When pyroptosis was assessed by measuring
229 LDH-release, *Gbp^{chr3-/-}*-deficient macrophages showed dramatically reduced cell death upon infection,
230 whereas the other mutant cells did not (**Figure 4B**). *Gbp^{chr3-/-}* macrophages did not exhibit increased
231 IFN-I production (**Figure 4C**), consistent with the notion that the GBPs are required for release of
232 bacterial LPS as well as DNA. These data suggested that GBPs contribute to both IFN-I-dependent and
233 IFN-I-independent killing of *R. parkeri*. Next, to assess the role for nitric oxide during *R. parkeri* infection,
234 we treated WT- and *Gbp^{chr3-/-}*-infected cells with IFN-I and the specific iNOS inhibitor L-NIL and monitored
235 bacterial growth. Upon iNOS inhibition, bacterial growth was increased in both WT and *Gbp^{chr3-/-}* cells
236 (**Figure 4D, 4E**). We also measured bacterial growth in IFN-I-treated *Nos2^{-/-}* BMDMs, but did not
237 observe any rescue in mutant versus WT cells (**Figure S4A**), but this result is complicated by the fact
238 that iNOS is a negative regulator of the NLRP3 inflammasome (Hernandez-Cuellar et al., 2012; Mishra
239 et al., 2013) and we observed more host cell death in *Nos2^{-/-}* BMDMs compared to WT cells (**Figure**
240 **S4B**). All together, these experiments reveal that the GBPs and perhaps nitric oxide are IRF5-regulated
241 genes that non-redundantly restrict *R. parkeri* growth in macrophages upon IFN-I treatment.

242 GBP-mediated killing of other pathogens has also been examined downstream of IFN- γ
243 treatment (Pilla-Moffett et al., 2016; Yamamoto et al., 2012). To assess the role of GBPs in IFN- γ -
244 dependent restriction of *R. parkeri*, bacterial growth was measured in WT and *Gbp^{chr3-/-}* cells in the
245 presence of different concentrations of IFN- γ . At lower concentrations of IFN- γ (0.2 ng/ml), we observed
246 a small but significant rescue in bacterial growth in *Gbp^{chr3-/-}* versus WT cells (**Figure 4F**). However,
247 higher concentrations of IFN- γ (4 ng/ml) ablated *R. parkeri* growth in both WT and *Gbp^{chr3-/-}* BMDMs
248 (**Figure 4F**). This revealed that IFN- γ potentially stimulates macrophages to kill *R. parkeri* by a mechanism
249 that partially depends on GBPs.

250 The GBPs have been observed to localize to the surface of intracellular pathogens at steady-
251 state conditions and upon the addition of interferons (Liu et al., 2018; Mitchell and Isberg, 2017;
252 Yamamoto et al., 2012). To determine if the GBPs localized to the surface of *R. parkeri*, we performed
253 immunofluorescence microscopy using a GBP2-specific antibody. GBP2 localized to the surface of ~1%
254 of bacteria in untreated WT cells at 3 hpi, and ~5% of total bacteria in IFN-I treated cells (**Figure 4G,**
255 **H**). No colocalization was observed in infected *Gbp^{chr3-/-}* macrophages, demonstrating that the antibody
256 is specific for the GBPs (**Figure S3**). Together, these data demonstrate that the GBPs localize to *R.*
257 *parkeri* and restrict bacterial growth at steady-state conditions, which is enhanced by IFN-I.

258

259 **In spleens, the inflammasome antagonizes the anti-rickettsial effects of IFN-I**

260 Our data from macrophages suggested a model for *R. parkeri* intracellular survival whereby
261 inflammasome activation antagonizes the anti-rickettsial activity of IFN-I. To determine whether this
262 pathway is important *in vivo*, we analyzed the role for the inflammasome, IFN-I, and IFN- γ in spleens of
263 infected mice, where *Rickettsia* spp. proliferate upon systemic infection (Feng et al., 1994). In
264 agreement with the data from macrophages *in vitro*, IFN- β mRNA was significantly upregulated in
265 spleens of infected *Casp1^{-/-}Casp11^{-/-}* mice when compared to WT mice, as measured by qPCR (**Figure**
266 **5A**). To determine if the increased IFN- β transcript abundance was dependent on cGAS, we also
267 measured IFN- β mRNA in infected *Casp1^{-/-}Casp11^{-/-}Cgas^{-/-}* mice, and observed a reduction in IFN- β
268 transcript abundance (**Figure 5A**). This demonstrated that the inflammasome antagonizes cGAS-
269 induced IFN-I *in vivo*, as it does *in vitro*.

270 To determine if the increased IFN-I observed in *Casp1^{-/-}Casp11^{-/-}* mice restricted *R. parkeri*, we
271 compared bacterial burdens between *Casp1^{-/-}Casp11^{-/-}* and *Casp1^{-/-}Casp11^{-/-}Ifnar^{-/-}* mice. The triple
272 *Casp1^{-/-}Casp11^{-/-}Ifnar^{-/-}* mutant showed a significantly increased bacterial burden in comparison to the
273 double *Casp1^{-/-}Casp11^{-/-}* mutant (**Figure 5B**). To ascertain if the increased bacterial growth was due to
274 cGAS-dependent IFN-I, we also measured bacterial burdens in *Casp1^{-/-}Casp11^{-/-}Cgas^{-/-}* mice, and
275 similarly observed increased bacterial burdens compared with the *Casp1^{-/-}Casp11^{-/-}* mutant (**Figure**
276 **5B**). It remains unclear why spleens of *Casp1^{-/-}Casp11^{-/-}* mice, which produce more IFN- β , do not have

277 reduced bacterial burdens when compared to WT (as in macrophages); nevertheless, these data reveal
278 that the mechanisms of *R. parkeri* growth in spleens is similar to macrophages *in vitro*, where bacterial
279 activation of the inflammasome limits the antimicrobial effects of cGAS-induced IFN-I.

280 In macrophages, we also observed a role for IFN- γ in restricting *R. parkeri* growth; however, the
281 role for IFN- γ and its relationship to the inflammasome during *Rickettsia* infection *in vivo* is unknown.
282 We therefore next assessed if IFN- γ restricted *R. parkeri* growth in the spleens of infected mice.
283 Neutralization of IFN- γ using an anti-IFN- γ antibody increased bacterial burdens in *Casp1^{-/-}Casp11^{-/-}*
284 mice 2.5-fold when compared to untreated *Casp1^{-/-}Casp11^{-/-}* mice, suggesting that IFN- γ restricts
285 bacterial growth (**Figure 5B**, right side of dotted line). To reveal if IFN- γ and IFN-I both control infection
286 in the spleen, we neutralized IFN- γ in infected *Casp1^{-/-}Casp11^{-/-}Ifnar^{-/-}* mice. This increased bacterial
287 burdens 51-fold over untreated *Casp1^{-/-}Casp11^{-/-}* mice (**Figure 5B**, right side of dotted line). These data
288 demonstrate that in spleens of WT mice, inflammasome activation limits protective IFN-I production,
289 and that IFN-I and IFN- γ both contribute to protection.

290

291 **In livers, the inflammasome antagonizes IFN-I, which in turn antagonizes the anti-bacterial**
292 **effects of IFN- γ**

293 We also measured bacterial burdens in the livers, where *Rickettsia* and other bacterial
294 pathogens also reside during infection (Feng et al., 1994; Rayamajhi et al., 2010). In contrast to what
295 was observed in spleens, infected *Casp1^{-/-}Casp11^{-/-}* mice had 15-fold higher bacterial burdens than WT
296 mice in the liver (**Figure 5C**). Also in contrast to what was observed in spleens, the bacterial burden in
297 infected *Casp1^{-/-}Casp11^{-/-}Ifnar^{-/-}* mice, as well as *Casp1^{-/-}Casp11^{-/-}Cgas^{-/-}* mice, was indistinguishable
298 from WT (**Figure 5C**), suggesting that the 15-fold increase observed in *Casp1^{-/-}Casp11^{-/-}* mice was
299 dependent on IFN-I. We hypothesized that this effect might be due to IFN-I antagonizing the anti-
300 bacterial effects of IFN- γ , as it was previously demonstrated that IFN-I antagonizes the effects of IFN- γ
301 in the liver during *L. monocytogenes* infection (Rayamajhi et al., 2010). To test whether IFN-I
302 antagonized the anti-rickettsial effects of IFN- γ , infected *Casp1^{-/-}Casp11^{-/-}* and *Casp1^{-/-}Casp11^{-/-}Ifnar^{-/-}*

303 mice were treated with the IFN- γ neutralizing antibody and bacterial burdens were measured. The
304 difference in bacterial burdens between these mice was erased upon IFN- γ neutralization (**Figure 5C**,
305 right), demonstrating that IFN-I was responsible for antagonizing IFN- γ . Together, these results suggest
306 that the inflammasome protects against *R. parkeri* infection in the liver, in part by limiting IFN-I
307 antagonism of IFN- γ (**Figure 5D**).

308

309 **Both IFN-I and IFN- γ are required to control *R. parkeri* infection in mice**

310 Because we observed that bacterial burdens in organs increased when both IFN-I and IFN- γ
311 were removed, we next tested whether these cytokines were protective at the whole animal level. We
312 infected C57BL/6 mice deficient for both IFN-I and IFN- γ receptors (*Ifnar*^{-/-}*Ifngr*^{-/-}) via the intravenous
313 route. Strikingly, whereas WT, *Ifnar*^{-/-}, and *Ifngr*^{-/-} mice survived an infectious dose of 10⁷ bacteria with
314 no severe symptoms, the majority of *Ifngr*^{-/-}*Ifnar*^{-/-} mice succumbed within 6 d (**Figure 6A**), and lost body
315 weight and had reduced body temperature over time (**Figure 6B,C**). Symptoms of infection were dose-
316 dependent. At a dose of 10⁶ bacteria, mice lost weight, their temperature decreased, and many
317 succumbed to infection, although some eventually recovered to their original body weight and
318 temperature. At dose of 10⁵ bacteria, none of the mice succumbed to infection, but the animals lost
319 weight and their body temperature decreased, which then recovered to pre-infection levels. We also
320 performed these experiments using AG129 mice, which are similarly mutated for *Ifngr* and *Ifnar*, but are
321 in a different genetic background. These mice were also highly susceptible to infection with 10⁷ bacteria,
322 with 100% fatality by 6 dpi (**Figure 6D**). Together, these data demonstrate that both IFN-I and IFN- γ
323 potently control *R. parkeri* growth in animals. The discovery of the sensitivity of this mouse genotype
324 reveals it as robust animal model for further investigations into pathogenesis of the SFG *Rickettsia*.

325

326 **Discussion**

327 Avoiding innate immunity is critical for microbial pathogens to survive and cause disease.
328 Whereas some facultative pathogens that inhabit the cytosol resist killing by IFN-I and avoid the

329 inflammasome, the innate immune response to obligate intracellular bacteria has remained largely
330 unexplored. We report the unexpected discovery that the innate immune response to the obligate
331 intracellular human pathogen *R. parkeri* is distinctive among other cytosolic pathogens, as the bacteria
332 are sensitive to IFN-I-mediated killing, but avoid stimulating a robust IFN-I response by exploiting the
333 inherent trade-off between inflammasome activation and IFN-I production.

334 We observed that *R. parkeri* were restricted by IFN-I in macrophages and in mice. Furthermore,
335 IFN-I much more potently restricted *R. parkeri* in macrophages than was previously seen for other
336 *Rickettsia* spp. in immortalized endothelial cells and fibroblasts (Colonne et al., 2011; Turco and
337 Winkler, 1990). In contrast, facultative cytosolic pathogens such as *L. monocytogenes* are resistant to
338 the killing effects of IFN-I in primary myeloid cells (Bauler et al., 2011; Woodward et al., 2010) and in
339 mice (Auerbuch et al., 2004; Rayamajhi et al., 2010). Given their sensitivity to IFN-I, we propose that
340 *Rickettsia* must have evolved mechanisms to avoid stimulating IFN-I production.

341 Our results suggest that one critical mechanism for avoiding IFN-I production is that *R. parkeri*-
342 induces pyroptosis, which dampens IFN-I production, protecting the remaining bacterial population that
343 has successfully infected other cells (**Figure 7**, left). In support of this conclusion, we observed that a
344 subpopulation of *R. parkeri* activated caspase-11 and GSDMD to cause pyroptosis. Because pyroptosis
345 is a rapid post-translational signaling event (Kayagaki et al., 2015), activation of this cell death pathway
346 prohibits IFN-I production, which is slower as it requires transcription, translation, and secretion. We
347 found that macrophages that are deficient for inflammasome signaling restricted *R. parkeri* because
348 bacterial ligands instead activated robust IFN-I production via cGAS, leading to bacterial killing (**Figure**
349 **7**, right). We also observed that the GBPs are required for pyroptosis and for IFN-I production in the
350 absence of host cell death. From these observations, we conclude that bacteriolysis is likely responsible
351 for the release of LPS and DNA that stimulate caspase-11 and cGAS. In contrast with what we observed
352 for *R. parkeri*, several facultative bacterial pathogens have evolved different mechanisms to avoid the
353 inflammasome (Jorgensen and Miao, 2015), including modification LPS by *F. novicida* to avoid
354 caspase-11 (Hagar et al., 2013; Wallet et al., 2016), downregulation of flagellin by *L. monocytogenes*
355 to avoid NAIP5 (Miao et al., 2010; Shen and Higgins, 2006), and infrequent lysis by *F. tularensis* and *L.*

356 *monocytogenes* to avoid AIM2 (Sauer et al., 2010; Ulland et al., 2010). We propose that inflammasome
357 activation is a trade-off that allows for growth of a pathogen that is sensitive to IFN-I.

358 Downstream of IFN-I production, we observed that the transcription factor IRF5 is critical for
359 restriction of *R. parkeri* in macrophages *in vitro*. IRF5 in turn upregulates the expression of anti-microbial
360 factors including the GBPs and iNOS, which protect against *R. parkeri*. These data agree with a
361 previously established role for nitric oxide in protecting against infection by other *Rickettsia* spp. in
362 mouse and human cells (Feng and Walker, 1993; 2000; Feng et al., 1994; Turco and Winkler, 1993;
363 Woods et al., 2005), although it remains unclear if nitric oxide directly or indirectly kills these pathogens.
364 These data also reveal an unappreciated role for the GBPs in rickettsial killing. We observed that iNOS
365 and GBPs acted additively and non-redundantly, and only partially account for the killing effects of IFN-
366 I. We suspect that additional IRF5-regulated genes contribute to controlling *R. parkeri* infection, and
367 identifying these factors will be critical for understanding how interferons control infection by obligate
368 pathogens.

369 Consistent with our observations in macrophages *in vitro*, we found that the inflammasome
370 antagonizes IFN-I production *in vivo*. However, we observed tissue-specific differences in the spleen
371 and liver with regard to the relative protective role for IFN-I. In the spleen, IFN-I protects against
372 infection. These data are in agreement with previously known roles for the inflammasome in the spleen,
373 where the major protective pathway elicited by the inflammasome is pyroptosis (Maltez et al., 2015).
374 Our observations expand on these previous findings, by revealing that an inherent trade-off of
375 pyroptosis is that it limits protective IFN-I in the spleen. However, in the liver, IFN-I enhances infection
376 due to its effects of antagonizing IFN- γ . These observations are also in agreement with a previous study
377 demonstrating that cytokine production is the more important facet of inflammasome activation in the
378 liver (Maltez et al., 2015), and expand on these studies by demonstrating that the inflammasome also
379 acts by antagonizing IFN-I. Our observations are also consistent with a study demonstrating that IFN-I
380 antagonizes IFN- γ in the liver, as observed during *L. monocytogenes* infection (Rayamajhi et al., 2010).
381 Moreover, our observations in both organs are consistent with earlier studies establishing a protective
382 role for IFN- γ during *Rickettsia* infection *in vivo* (Feng et al., 1994; Li et al., 1987). Based on our findings

383 that IFN-I and IFN- γ act differently in the spleen and liver, we speculate that interferons may pressure
384 pathogens to evolve organ-specific tropisms to accommodate their intracellular lifestyle.

385 In keeping with our observations that IFN-I and IFN- γ restrict *R. parkeri* growth in macrophages
386 *in vitro*, we observed that *Ifnar*^{-/-}*Ifngr*^{-/-} mice rapidly succumbed to infection. These findings demonstrate
387 that both types of interferon play a critical role in protecting against *R. parkeri* infection. Our observations
388 are also of strong practical importance, as this mouse exhibits a pathology that makes it a useful animal
389 model for future studies examining the bacterial determinants that contribute to SFG *Rickettsia*
390 pathogenesis and for evaluating the impacts of infection at the organ, tissue and cellular levels *in vivo*.
391 Future studies will aim to characterize facets of infection including dissemination, vascular damage, as
392 well as the innate immune response.

393 Our data suggest that obligate cytosolic pathogens such as *R. parkeri* may occupy an
394 intermediate position in the spectrum between bacteria and viruses, both with regard to their
395 dependency on the host and their interplay with the innate immune system (**Figure 7B**). For example,
396 during infection with *R. parkeri* as well as with herpes simplex virus 1 or Vaccinia virus, activation of the
397 inflammasome antagonizes the protective IFN-I response (Wang et al., 2017). Additionally, IRF5 is
398 required for controlling *R. parkeri* and viral infection (Carlin et al., 2017; Proenca-Modena et al., 2016;
399 Thackray et al., 2014). Lastly, as with *R. parkeri*, many viruses have increased lethality in *Ifnar*^{-/-}*Ifngr*^{-/-}
400 mice (Milligan et al., 2017; Rossi et al., 2016), suggesting a non-redundant protective role for IFN-I and
401 IFN- γ in both types of infection. These similarities are not true for facultative cytosolic bacterial
402 pathogens such as *L. monocytogenes*, for which IFN- γ is significantly more protective than IFN-I
403 (Rayamajhi et al., 2010). Our observations regarding the interaction between *R. parkeri* and innate
404 immune pathways underscores the notion that obligate pathogens have evolved different strategies
405 than facultative pathogens to fit their ecological niche. Their ability to tolerate inflammasome activation
406 to avoid IFN-I is an evolutionary strategy that may be shared among obligate microbes, whose complete
407 reliance on host cell metabolic and cellular pathways for survival may also dispose them to IFN-I
408 sensitivity. Continued investigation of the interaction between obligate intracellular bacteria and innate

409 immunity will enhance our understanding of how pathogens exploit host cell immunity to survive and to
410 cause disease.

411

412 **Acknowledgements**

413 We thank Dr. Mike Diamond (Washington University, St. Louis) for femurs from *Irf5*^{-/-}, *Ifit1*^{-/-}, and
414 *Ifit2*^{-/-} mice. We thank Dr. Daniel Rader (Pittsburg University) for femurs from *LipG*^{-/-} mice. We thank Dr.
415 Jörn Coers (Duke University) and Dr. Masahiro Yamamoto (Osaka Yamamoto) for femurs from *Gbp*^{chr3-}
416 ^{-/-} mice. We thank Dr. Eva Harris (UC Berkeley) for AG129 mice (originally obtained from M. Aguet,
417 Swiss Institute for Experimental Research, Epalinges, Switzerland). We thank Dr. Greg Barton (UC
418 Berkeley) for helpful advice and for *Irf3*^{-/-}*Irf7*^{-/-} mice and *Tnfrsf1a*^{-/-}*Tnfrsf1b*^{-/-} mice. We thank Neil Fischer
419 for critical reading of this manuscript. P.E. was supported by postdoctoral fellowships from the
420 Foundation Olle Engkvist Byggmästare, the Swedish Society of Medical Research (SSMF), and the
421 Sweden-America Foundation. M.D.W. was supported by NIH/NIAID grants R01 AI109044, R21
422 AI109270, and R21 AI138550. R.E.V. is an HHMI investigator and is supported by NIH/NIAID grants
423 AI075039 and AI063302.

424

425 **Author contributions**

426 Conceptualization: T.P.B; Methodology: T.P.B., P.E.; Investigation: T.P.B., P.E., and R.C.;
427 Visualization: T.P.B., P.E., R.E.V., and M.D.W.; Writing: Original Draft, T.P.B.; Writing – Review &
428 Editing, T.P.B., P.E., R.E.V., and M.D.W.; Funding Acquisition, R.E.V. and M.D.W.; Resources, R.E.V.
429 and M.W.D.; Supervision, R.E.V. and M.D.W.

430

431 **Declaration of interests**

432 The authors declare no conflicts of interest.

433

434 **Figure Legends**

435 **Figure 1: Inflammasome activation promotes *R. parkeri* pathogenesis by antagonizing the IFN-I**
436 **response in macrophages**

437 **A)** Measurement of *Rickettsia parkeri* (*Rp*) PFU in BMDMs over time. WT BMDMs were infected in a
438 24-well plate at an MOI of 0.2. MOI was calculated based on the ratio of the number of infectious
439 bacteria, as determined by plaque assay, to the number of BMDMs. At each time point, BMDMs were
440 lysed with water and lysates were plated over a confluent monolayer of Vero cells. Recombinant IFN- β
441 (PBL, 12405-1) was added at 0 hpi. U signifies units of recombinant IFN- β . Statistical comparisons were
442 made between each sample and untreated cells at each time point. Data are a compilation of at least
443 two separate experiments and are expressed as means \pm SEM. **B)** Measurement of *Listeria*
444 *monocytogenes* (*Lm*) CFU in BMDMs. WT BMDMs were infected in 24-well plate at an MOI of 1. MOI
445 was calculated based on the ratio of bacteria in liquid culture to BMDMs. 3,000 U of recombinant IFN-
446 β (PBL, 12405-1) was added at 0 hpi. Data are the combination of at least two separate experiments
447 and are expressed as means \pm SEM. **C)** Measurement of IFN-I in supernatants of cells infected with *R.*
448 *parkeri* or *L. monocytogenes*. WT BMDMs were infected with *R. parkeri* or *L. monocytogenes* at an MOI
449 of 1 and supernatants were harvested at 8 hpi for *L. monocytogenes* and 24 hpi for *R. parkeri*.
450 Supernatants were used to stimulate a luciferase-expressing cell line and relative light units (RLU) were
451 measured and compared between each sample and uninfected cells. Statistical comparisons were
452 made between each sample and infected WT cells. Data are the compilation of at least two separate
453 experiments and are expressed as means \pm SEM. **D)** Quantification of host cell death during *R. parkeri*
454 infection of BMDMs. LDH release was measured at 24 hpi upon *R. parkeri* infection at an MOI of 1.
455 Statistical comparisons were made between each sample and WT B6 cells. Data are the compilation of
456 at least three separate experiments and are expressed as means \pm SEM. **E)** Images of BMDMs infected
457 with *R. parkeri*. Cells were infected at an MOI of 1 and images were captured at 96 hpi. The scale bar
458 is 100 μ m. **F)** Measurement of the number of infectious *R. parkeri* in BMDMs over time. BMDMs were
459 infected with *R. parkeri* at an MOI of 1 and PFU were determined every 24 hpi. Statistical comparisons
460 were made between each sample and WT B6 cells at each time point. Data are the compilation of at
461 least three separate experiments and are expressed as means \pm SEM. **G)** Measurement of the number

462 of infectious *R. parkeri* in BMDMs over time. Cells were infected with *R. parkeri* at an MOI of 0.2 and
463 PFU were measured over time. Statistical comparisons were made between each sample and WT B6
464 cells at each time point. Data are the compilation of at least three separate experiments and are
465 expressed as means \pm SEM. “Supe” indicates supernatant collected at 24 hpi from *Casp1^{-/-}Casp11^{-/-}*
466 BMDMs infected with *R. parkeri* at an MOI of 1. **H)** Measurement of IFN-I in supernatants of cells
467 infected with *R. parkeri*. Supernatants from infected cells were harvested at 24 hpi and used to stimulate
468 a luciferase-expressing cell line and relative light units (RLU) were compared between each sample
469 and uninfected cells. Statistical comparisons were made between each sample and infected WT cells.
470 Data are the compilation of at least three separate experiments and are expressed as means \pm SEM.
471 **I)** Measurement of the number of infectious *R. parkeri* in BMDMs over time. Cells were infected at an
472 MOI of 1 and PFU were measured over time. The α -IFNAR antibody was added at T=0 to a final
473 concentration of 1 μ g/ml. Statistical comparisons were made between each sample and WT B6 cells at
474 each time point. Statistical analyses for data in panels A, B, C, F, G, and I were performed using a two-
475 tailed Student’s T-test, where each sample at each time point was compared to the control. Statistical
476 analyses in panels D and H were performed using an ANOVA with multiple comparisons post-hoc test.
477 *p<0.05, **p<0.01, ***p<0.001, ****p<0.0001, ns=not significant.

478

479 **Figure 2: Pyroptosis masks cGAS-induced IFN-I**

480 **A)** Quantification of host cell death during *R. parkeri* infection of BMDMs. LDH release was measured
481 at 24 hpi upon *R. parkeri* infection of the indicated BMDMs at an MOI of 1. Statistical comparisons were
482 made between each sample and WT B6 cells. Data are the compilation of at least three separate
483 experiments and are expressed as means \pm SEM. **B)** Measurement of IFN-I abundance in supernatants
484 of infected BMDMs. The indicated BMDMs were infected with *R. parkeri* at an MOI of 1. Supernatants
485 from infected cells were harvested at 24 hpi and used to stimulate a luciferase-expressing cell line and
486 compared to uninfected cells. Statistical comparisons were made between each sample and infected
487 WT cells. Data are a compilation of at least three separate experiments and are expressed as means
488 \pm SEM. **C)** Measurement of bacterial PFU in BMDMs over time. BMDMs were infected with *R. parkeri*

489 at an MOI of 1 and PFU were measured over time. Statistical comparisons were made between each
490 sample and WT B6 cells at each time point. Data are the compilation of at least three separate
491 experiments and are expressed as means \pm SEM. Statistical analyses for bacterial abundance in panel
492 C were performed using a two-tailed Student's T-test, where each sample at each time point was
493 compared to the control. Statistical analyses for LDH assays and IFN-I abundance in panels A and B
494 were performed using an ANOVA with multiple comparisons post-hoc test. * $p < 0.05$, ** $p < 0.01$,
495 *** $p < 0.001$, **** $p < 0.0001$, ns=not significant.

496
497 **Figure 3: IRF5 is required for IFN-I-dependent restriction of *R. parkeri***

498 **A)** Measurement of *R. parkeri* PFU in BMDMs over time. Cells were infected at an MOI of 0.2, and
499 PFU were measured over time. 10,000 units of recombinant IFN- β (rIFN- β) was added at 0 hpi.
500 Statistical comparisons were made between each sample and untreated cells at each time point. Data
501 are the compilation at least three separate experiments and are expressed as means \pm SEM. **B)**
502 Measurement of bacterial PFU in BMDMs. Cells were infected at an MOI of 1, and PFU were measured
503 over time. Statistical comparisons were made between each sample and WT B6 cells at each time
504 point. Data are the compilation at least three separate experiments and are expressed as means \pm
505 SEM. "Supe" indicates 200 μ l of supernatant collected at 24 hpi from *Casp1^{-/-}Casp11^{-/-}* BMDMs infected
506 with *R. parkeri* at an MOI of 1. All statistical analyses were performed using a two-tailed Student's T-
507 test. * $p < 0.05$, ** $p < 0.01$, *** $p < 0.001$, **** $p < 0.0001$, ns=not significant. **C)** Transcript abundance of
508 antimicrobial genes upregulated by IFN-I. BMDMs were infected at an MOI of 2.3, treated with 10,000
509 U recombinant IFN- β , and RNA was harvested at 12 hpi. High-throughput RNA-sequencing was then
510 performed. The regulation of 7 candidate anti-rickettsial genes is shown. Genes are ordered from
511 highest to lowest in terms of upregulation by IFN- β in WT cells, with the exception of *Nos2*, which is
512 shown separately because it was more highly regulated by IRF1 than IRF5. Each data set was
513 normalized to *R. parkeri*-infected WT, IFN- β -untreated BMDMs.

514

515 **Figure 4: The GBPs contribute to IFN-I-dependent and -independent inhibition of *R. parkeri***
516 **growth**

517 **A)** Measurement of *R. parkeri* PFU in BMDMs. BMDMs were infected with *R. parkeri* at an MOI of 0.2
518 and PFU were measured over time. “Supe” signifies 500 μ l supernatant from infected *Casp1^{-/-}Casp11^{-/-}*
519 *^* cells, which was added at 0 hpi. Statistical comparisons were made between each sample and
520 untreated cells at each time point. Data represent at least three separate experiments and are
521 expressed as means \pm SEM. **B)** Quantification of host cell death. LDH release was measured at 24 hpi
522 upon *R. parkeri* infection at an MOI of 1. Statistical comparisons were made between each sample and
523 WT B6 cells. Data are the compilation at least three separate experiments and are expressed as means
524 \pm SEM. **C)** Measurement of IFN-I abundance in supernatants of infected BMDMs. The indicated BMDMs
525 were infected with *R. parkeri* at an MOI of 1. Supernatants from infected cells were harvested at 24 hpi
526 and used to stimulate a luciferase-expressing cell line and compared to uninfected cells. Data are a
527 compilation of at least five separate experiments. **D,E,F)** Measurement of bacterial PFU in BMDMs.
528 Cells were infected at an MOI of 0.2, and PFU were measured over time. “Supe” signifies 500 μ l
529 supernatant from infected *Casp1^{-/-}Casp11^{-/-}* cells, which was added at 0 hpi. L-NIL was resuspended in
530 water and added to a final concentration of 1 mM at T=0. IFN- γ was added at 0 hpi. Statistical
531 comparisons were made between each sample and untreated cells at each time point. Data are the
532 compilation of at least three separate experiments and are expressed as means \pm SEM. **G)** A
533 representative image of GBP2 localization to the surface of *R. parkeri*. WT BMDMs were infected at an
534 MOI of 1, and were imaged at 3 hpi using 100x confocal immunofluorescence microscopy. Cyan staining
535 is phalloidin; green staining is α -GBP2 (ProteinTech); red staining is α -*Rickettsia*. The red and green
536 channels of the indicated white box are increased in size and shown on the right and bottom left. The
537 scale bar is 5.6 μ m. **H)** Quantification of GBP2 localization to the surface of *R. parkeri*. WT BMDMs
538 were infected at an MOI of 1, and were imaged at 3 hpi using 100x confocal immunofluorescence
539 microscopy. For IFN- β treated cells, BMDMs were treated overnight with 100 U recombinant IFN- β .
540 Each data point represents an individual experiment, and each experiment consists of at least 10
541 separate images, and each image contained approximately 20 bacteria. Statistical analyses for panels

542 A, C, D, E, F, and H were performed using a two-tailed Student's T-test, where each sample at each
543 time point was compared to the control. Statistical analyses for LDH assays in panel B were performed
544 using an ANOVA with multiple comparisons post-hoc test. * $p < 0.05$, ** $p < 0.01$, *** $p < 0.001$, **** $p < 0.0001$,
545 ns=not significant.

546

547 **Figure 5: In mice, inflammasome activation antagonizes IFN-I production, leading to tissue-**
548 **specific effects on *R. parkeri* burdens**

549 **A)** Measurement of IFN- β transcripts in infected mice. C57BL/6 mice were infected i.v. with 10^7 *R.*
550 *parkeri*, and qPCR was used to analyze IFN- β and actin transcript abundance at 72 hpi in spleens. IFN-
551 β was normalized to actin to determine relative copy number per mouse spleen. Data are the
552 combination of at least 3 separate experiments. **B)** Measurement of bacterial burdens in mouse spleens.
553 Mice were infected i.v. with 10^7 *R. parkeri*, and bacterial burdens were determined in spleens at 72 hpi
554 via plaque assay. Colors were arbitrarily assigned to distinguish between genotypes. Data are the
555 combination of at least 3 separate experiments. Statistical analyses were performed using Mann-
556 Whitney U test. Bars denote medians. **C)** Measurement of bacterial burdens in mouse livers. Mice were
557 infected i.v. with 10^7 *R. parkeri* and bacterial burdens were determined in livers at 72 hpi via plaque
558 assay. For α -IFN- γ (BioLegend), mice were injected i.v. with 300 μ l at 30 minutes postinfection (mpi),
559 200 μ l at 24 hpi, and 200 μ l at 48 hpi, totaling 800 μ l (0.8 μ g antibody). Colors are used to distinguish
560 between genotypes. Data are the combination of at least 3 separate experiments, with the exception of
561 experiments using the α -IFN- γ antibody, which are a combination of 2 separate experiments. Statistical
562 analysis performed for qPCR experiments in panel A used a two-tailed Student's T Test. Statistical
563 analyses for *in vivo* experiments in panels B and C were performed using a Mann-Whitney U test. Bars
564 denote medians. * $p < 0.05$, ** $p < 0.01$, *** $p < 0.001$, **** $p < 0.0001$, ns=not significant. **D)** Textual summary
565 of results from *in vivo* infections.

566

567 **Figure 6: Mice mutated for both *Ifnar* and *Ifngr* succumb to *R. parkeri* infection**

568 **A)** Survival of mice lacking interferon signaling. Mice in the C57BL/6 background were infected i.v. with
569 the indicated concentrations of *R. parkeri*, and survival was measured over time. Mice were euthanized
570 if their core body temperature fell below 90° F or if they exhibited symptoms of severe infection, such
571 as severe hunching, scruffing, or inability to move around the cage. Infections from at least 6 mice are
572 shown for each genotype. Data are the combination of at least three separate experiments. **B)**
573 Measurement of mouse weight during infection. Mice were infected with 10^7 *R. parkeri* and weight was
574 measured every 24 hpi. Data are normalized to the weight starting at the initial time of infection. **C)**
575 Measurement of mouse core body temperature during infection. Mice were infected with 10^7 *R. parkeri*
576 and body temperature was measured every 24 hpi, using a rectal thermometer. **D)** Survival of mice
577 lacking interferon signaling. Mice of the 129 genotype lacking IFN-I and IFN- γ receptors (AG129) were
578 infected i.v. with the indicated concentrations of *R. parkeri* and mouse health was measured over time.
579 Mice were euthanized if their core body temperature fell below 90° F or if they exhibited symptoms of
580 severe infection. At least 6 mice were used for each condition. Data are the combination of at least 3
581 separate experiments.

582

583 **Figure 7: Inflammasome-mediated antagonism of IFN-I promotes intracellular growth of *R.***
584 ***parkeri***

585 **A)** Model depicting intracellular growth of *R. parkeri* in WT cells (left) or in cells lacking inflammasome
586 signaling (right). **B)** Visual representation of the antimicrobial effects of interferons on cytosolic
587 pathogens. Red zones indicate approximate restrictive effects of interferons.

588

589 **STAR Methods**

590 **Contact for reagent and resource sharing**

591 Further information and requests for reagents may be directed to and will be fulfilled by the Lead
592 Contact Dr. Matthew D. Welch (welch@berkeley.edu).

593

594 **EXPERIMENTAL MODEL AND SUBJECT DETAILS**

595 **Bacterial strains**

596 All *R. parkeri* used in this study were in the Portsmouth strain originally obtained from
597 Christopher Paddock (Centers for Disease Control and Prevention) and were authenticated by whole
598 genome sequencing (NCBI Trace and Short-Read Archive; Sequence Read Archive (SRA), accession
599 number SRX4401164). To prepare the bacteria for infections, confluent T175 flasks of female African
600 green monkey kidney epithelial Vero cells (authenticated by STR analysis) grown in DMEM (Gibco
601 11965-092) with glucose (4.5 g/L) supplemented with 2% fetal bovine serum (FBS, GemCell) were
602 infected with 5×10^6 *R. parkeri* per flask and rocked for 10 min at 37°C. Infected cells were scraped and
603 collected at 5-6 dpi when ~90% of cells were highly infected, as indicated by cell rounding. Scraped
604 cells were centrifuged at 12,000 x G for 20 min at 4°C. Pelleted cells were then resuspended in K-36
605 buffer (0.05 M KH₂PO₄, 0.05 M K₂HPO₄, 100 mM KCl, 15 mM NaCl, pH 7) and transferred to a cold
606 glass Dounce homogenizer. Bacteria were released from infected cells by repeated douncing (60
607 strokes). The dounced solution was then centrifuged at 200 x G for 5 min at 4°C to pellet host cell debris.
608 The supernatant containing *R. parkeri* was overlaid on a 30% MD-76R (Merry X-Ray) solution.
609 Gradients were then centrifuged at 18,000 rpm in an SW-28 ultracentrifuge swinging bucket rotor
610 (Beckman/Coulter) for 20 min at 4°C to separate remaining host cells debris from the bacteria. Bacterial
611 pellets were resuspended in brain heart infusion (BHI) media (BD, 237500) and stored at -80°C.

612 Titers were determined for *R. parkeri* stocks via plaque assays by serially diluting the bacteria
613 in 6-well plates containing confluent Vero cells, which were plated ~24 h prior. Plates were then spun
614 for 5 min at 300 x G in an Eppendorf 5810R centrifuge. At 24 hpi, the media from each well was
615 aspirated and the wells were overlaid with 4 ml/well DMEM with a final concentration of 5% FBS and
616 0.7% ultrapure agarose (Invitrogen, 16500-500). When plaques were visible at 5-6 dpi, an overlay of
617 0.7% agarose in DMEM containing 2.5% neutral red solution (Sigma, N6264) was added and plates
618 incubated overnight until plaques were clearly visible. Plaques were then counted to determine bacterial
619 concentrations.

620 *L. monocytogenes* strain 10403S was originally obtained from Dr. Daniel Portnoy (UC Berkeley).

621

622 **Animal experiments**

623 Animal research using mice was conducted under a protocol approved by the UC Berkeley
624 Institutional Animal Care and Use Committee (IACUC) in compliance with the Animal Welfare Act and
625 other federal statutes relating to animals and experiments using animals. The UC Berkeley IACUC is
626 fully accredited by the Association for the Assessment and Accreditation of Laboratory Animal Care
627 International and adheres to the principles of the Guide for the Care and use of Laboratory Animals.
628 Infectious disease studies were performed in a biosafety level 2 facility. All animals were maintained at
629 the UC Berkeley campus and all infections were performed in accordance with the approved Welch lab
630 Animal Use Protocol. Mice were age matched between 8 and 18 weeks old. Mice were selected for
631 experiments based on their availability, regardless of sex. PFU data for each gender is reported in
632 **Figure S5** at 48 and 72 hpi. All mice were healthy at the time of infection and were housed in
633 microisolator cages and provided chow and water. Experimental groups were littermates of the same
634 sex that were randomly assigned to experimental groups. All mice were phenotypically healthy at the
635 time of the experiment, as determined by their weight, temperature, and movement around the cage.
636 For experiments with mice mutated for *Ifnar* and *Ifngr*, as described in Figure 6, mice were immediately
637 euthanized if they exhibited severe degree of infection, as defined by a core body temperature dropping
638 below 90° F or lethargy that prevented the mouse from moving around the cage normally.

639

640 **Mouse genotyping**

641 *Casp1*^{-/-} (Rauch et al., 2017), *Sting*^{gt/gt} (Sauer et al., 2011), *Cgas*^{-/-} (Marcus et al., 2018), *Gsdmd*^{-/-}
642 (Rauch et al., 2017), *Irf5*^{-/-} (Purtha et al., 2012), *Ifit1*^{-/-} (Szretter et al., 2012), and *Ifit2*^{-/-} (Fensterl et al.,
643 2012), *lipG*^{-/-} (Ishida et al., 2003), *Gbp*^{chr3-/-} (Yamamoto et al., 2012) mice were previously described.
644 *Casp11*^{-/-} (Wang et al., 1998), *Irf1*^{-/-} (Matsuyama et al., 1993), *Ifnar*^{-/-} (Müller et al., 1994), *Ifngr*^{-/-} (Huang
645 et al., 1993), *Ifnar*^{-/-}*Ifngr*^{-/-}, and WT mice were previously described and originally obtained from Jackson
646 Laboratories. For genotyping, ear clips were boiled for 15 min in 60 µl of 25 mM NaOH, quenched with
647 10 µl tris-HCl pH 5.5, and 2 µl of lysate was used for PCR using SapphireAMP (Takara, RR350) and
648 primers specific for each gene. Mutant mice were genotyped using the following primers: *Ifnar* forward

649 (F): CAACATACTACAACGACCAAGTGTG; *Ifnar* WT reverse (R): AACAAACCCCCAAACCCCAG;
650 *Ifnar* mutant R: ATCTGGACGAAGAGCATCAGG; WT *Casp1/11* F: CATGCCTGAATAATGATCACC;
651 WT *Casp1/11* R: GAAGAGATGTTACAGAAGCC; *Casp1/11* mutant F: GCGCCTCCCCTACCCGG;
652 *Casp1/11* mutant R: CTGTGGTGACTAACCGATAA; *Cgas* F: ACTGGGAATCCAGCTTTTCACT; *Cgas*
653 R: TGGGGTCAGAGGAAATCAGC; WT *tlr4* F: CACCTGATACTTAATGCTGGCTGTAAAAAG; WT *tlr4*
654 R: GGTTAGGCCCCAGAGTTTTGTTCTTCTCA; *tlr4* mutant F:
655 TGTTGCCCTTCAGTCACAGAGACTCTG; *tlr4* mutant R: TGTTGGGTCGTTTGTTCGGATCCGTCG;
656 *Sting* F: GATCCGAATGTTCAATCAGC; *Sting* R: CGATTCTTGATGCCAGCAC; *Gsdmd* F:
657 ATAGAACCCGTGGAGTCCCA; and *Gsdmd* R: GGCTTCCCTCATTCAGTGCT.

658

659 **Deriving bone marrow macrophages**

660 To obtain bone marrow, male or female mice were euthanized and femurs, tibiae, and fibulas
661 were excised. Visible muscle and connective tissue were removed from the bones and the bones were
662 sterilized with 70% ethanol. Bones were washed with BMDM media (20% HyClone FBS, 1% sodium
663 pyruvate, 0.1% β -mercaptoethanol, 10% conditioned supernatant from 3T3 fibroblasts, in Gibco DMEM
664 containing glucose and 100 U/ml penicillin and 100 ug/ml streptomycin) and ground using a mortar and
665 pestle. Bone homogenate was passed through a 70 μ m nylon Corning Falcon cell strainer (Thermo
666 Fisher Scientific, 08-771-2) to remove particulates. Filtrates were centrifuged in an Eppendorf 5810R at
667 1,200 RPM (290 x G) for 8 min, supernatant was aspirated, and the remaining pellet was resuspended
668 in BMDM media. Cells were then plated in non-TC-treated 15 cm petri dishes (at a ratio of 10 dishes
669 per 2 femurs) in a volume of 30 ml BMDM media and incubated at 37° C. An additional 30 ml BMDM
670 media was added 3 d later. At 7 d the media was aspirated and cells were incubated at 4° C with 15 ml
671 cold PBS (Gibco, 1x pH 7.4, no ions) for 10 min. BMDMs were then scraped from the plate, collected
672 in a 50 ml conical tube, and centrifuged at 1,200 RPM (290 x G) for 5 min. The PBS was then aspirated,
673 cells were resuspended in BMDM media, and cell numbers were counted using trypan blue and a
674 hemocytometer. For freezing, the pellet was resuspended in BMDM media with 30% FBS and 10%

675 DMSO at 10^7 cells/ml. 1 ml aliquots were frozen in a Styrofoam box at -80°C for one day and then
676 moved to liquid nitrogen.

677 **METHOD DETAILS**

678 **Mouse infections**

679 For mouse infections, *R. parkeri* were prepared by diluting 30%-prep bacteria to 1 ml cold sterile
680 PBS, centrifuging the bacteria at 12,000 x G for 1 min (Eppendorf 5430 centrifuge), and resuspended
681 in cold sterile PBS to the desired concentration (either 5×10^7 PFU/ml, 2.5×10^7 PFU/ml, 5×10^6 PFU/ml,
682 or 5×10^5 PFU/ml). Bacterial suspensions were kept on ice for the duration of the injections. For i.v.
683 injections, mice were exposed to a heat lamp while in their cages for approximately 5 minutes and then
684 each mouse was moved to a mouse restrainer (Braintree, TB-150 STD). The tail was sterilized with
685 70% ethanol and then 200 μl of bacterial suspensions were injected using 30.5 gauge needles into the
686 lateral tail vein. For monitoring body temperatures of infected mice, mice were placed in a mouse
687 restrainer, and a rodent rectal thermometer (BrainTree Scientific, RET-3) was used to measure
688 temperature. For delivering the anti-IFN- γ antibody (BioLegend, 505847), mice were injected i.v. with
689 300 μl at 30 min p.i., 200 μl at 24 hpi, and 200 μl at 48 hpi, totaling 800 μl (0.8 μg antibody). Mice were
690 monitored daily for clinical signs of disease, such as hunched posture, lethargy, or scruffed fur. Only
691 mice lacking both interferon receptors exhibited such symptoms of disease, and if this occurred, mice
692 were monitored daily for these symptoms, as well as for loss in body weight and temperature. If a mouse
693 displayed severe symptoms of infection, as defined by a reduction in body temperature below 90°F or
694 an inability to move around the cage normally, the animal was immediately and humanely euthanized
695 using CO_2 followed by cervical dislocation, according to IACUC-approved procedures.

696 For harvesting organs, mice were euthanized at the indicated pre-determined times and doused
697 with ethanol. Mouse organs were extracted in a biosafety cabinet and deposited into 50 ml conical tubes
698 (Falcon) containing 4 ml sterile cold PBS (Gibco 10010-023, no ions) for the spleen, and containing 8
699 ml cold sterile PBS for the liver. Organs were kept on ice and were each homogenized for approximately
700 10 s using an immersion homogenizer (Fisher, Polytron PT 2500E) at 22,000 RPM. Organ

701 homogenates were spun at 290 x G for 5 min to pellet cell debris (Eppendorf 5810R centrifuge). 20 μ l
702 of organ homogenates were plated into confluent Vero cells (plated 48 h prior) in 12-well plates, and
703 then serially diluted. The plates were then spun at 260 x G for 5 min at room temperature (Eppendorf
704 5810R centrifuge) and incubated at 33°C overnight. To reduce the possibility of contamination, organ
705 homogenates were plated in duplicate and the second replicate was treated with 50 μ g/ml carbenicillin
706 (Sigma) and 200 μ g/ml amphotericin B (Gibco). The next day, at approximately 16 hpi, the cells were
707 gently washed by replacing the existing media with 1 ml DMEM containing 2% FBS. The media was
708 then aspirated and replaced with 2 ml/well of DMEM containing 0.7% agarose, 5% FBS, and 200 μ g/ml
709 amphotericin B. When plaques were visible, at approximately 6 dpi, 1 ml of DMEM containing 0.7%
710 agarose, 1% FBS, and 2.5% neutral red (Sigma) was added to each well. Plaques were counted 24 h
711 later.

712

713 **Infections *in vitro***

714 Aliquots of BMDMs were thawed on ice, diluted into 9 ml of DMEM, centrifuged in an Eppendorf
715 5810R at 1,200 RPM (290 x G) for 5 minutes, and the pellet was resuspended in 10 ml BMDM media
716 without antibiotics. The number of cells was counted using Trypan blue (Sigma, T8154) and a
717 hemocytometer (Bright-Line), and 5×10^5 cells were plated into 24-well plates. Approximately 16 h later,
718 30% prep *R. parkeri* were thawed on ice and diluted into fresh BMDM media to the desired concentration
719 (either 10^6 PFU/ml or 2×10^5 PFU/ml). Media was then aspirated from the BMDMs, replaced with 500 μ l
720 media containing *R. parkeri*, and plates were spun at 300 G for 5 min in an Eppendorf 5810R. Infected
721 cells were then incubated in a humidified CEDCO 1600 incubator set to 33°C and 5% CO₂ for the
722 duration of the experiment.

723 For measuring PFU, supernatants were aspirated from individual wells, and each well was
724 gently washed twice with 500 μ l sterile milli-Q-grade water. 1 ml of sterile milli-Q water was then added
725 to each well and repeatedly pipetted up and down to lyse the host cells. Serial dilutions of lysates were
726 added to confluent Vero cells in 12 well plates that were plated 24 or 48 h prior. Plates were then spun
727 at 300 x G using an Eppendorf 5810R centrifuge for 5 min at room temperature and incubated at 33°C

728 overnight. At ~16 hpi, media was aspirated and replaced with 2 ml/well of DMEM containing 0.7%
729 agarose and 5% FBS. When plaques were visible, at approximately 6 dpi, 1 ml of DMEM containing
730 0.7% agarose, 1% FBS, 200 µg/ml amphotericin B (Invitrogen, 15290-018), and 2.5% neutral red
731 (Sigma) was added to each well. Plaques were counted 24 h later. For neutralizing IFN-I signaling, an
732 ultra-LEAF-purified α-IFNAR-1 antibody (BioLegend, 127323) was added to a final concentration of 1
733 µg/ml at 0 hpi. For experiments with recombinant TNF-α, 200 ng was added to each well in a 24-well
734 plate, and products from two different vendors were tested (BioLegend 575202 and Thermo PMC3014).

735 For collecting supernatant from *Casp1^{-/-}Casp11^{-/-}* cells, 5x10⁵ BMDMs in 24-well plates were
736 infected with *R. parkeri* at an MOI of 1 and at 24 hpi supernatants were pooled and stored at -80°C. For
737 adding the supernatant to infected BMDMs, either 200 or 500 µl of supernatant was removed at 20 mpi
738 from the untreated cells and replaced with the supernatant from *Casp1^{-/-}Casp11^{-/-}* cells.

739 For infections with *L. monocytogenes*, cultures of *L. monocytogenes* strain 10403S were grown
740 in 2 ml sterile-filtered BHI shaking at 37° until stationary phase (~16 h). Cultures were centrifuged at
741 20,000 x G (Eppendorf 5430), the pellet was resuspended in sterile PBS (Gibco 10010-023), and diluted
742 100-fold in PBS. 10 µl of the diluted bacteria were then added to each well of a 24-well plate of BMDMs
743 that were plated ~16 h prior to infections at 5x10⁵ cells/well. Bacteria were also plated out onto Luria
744 Broth agarose plates to determine the titer, which was determined to be ~5 x 10⁵ bacteria / 10 µl, for an
745 MOI of 1 (based on the ratio of bacteria in culture to number of BMDMs). Infected cells were incubated
746 in a humidified 37° incubator with 5% CO₂. 25 µg of gentamicin (Gibco 15710-064) was added to each
747 well (final concentration 50 µg/ml) at 1 hpi. At 30 mpi, 2, 5, and 8 hpi, the supernatant was aspirated
748 from infected cells, and cells were washed twice with sterile milli-Q water. Infected BMDMs were then
749 lysed with 1 ml sterile water by repeated pipetting and scraping of the well. Lysates were then serially
750 diluted and plated on LB agar plates, incubated at 37° overnight, and CFU were counted at ~20 h later.

751

752 **High-throughput DNA sequencing**

753 For high-throughput DNA sequencing, 5 x 10⁵ BMDMs were plated in 24-well plates and infected
754 16 h later with *R. parkeri* and treated with 10,000 activity units of recombinant IFN-β (PBL Cat # 12405-

755 1). To determine the percentage of cells that were successfully infected, we analyzed the infected cells
756 using immunofluorescence microscopy and observed that the multiplicity of infection (the average
757 number of bacteria per host cell) was 2.3, and that 71% of cells were infected. At 12 hpi, cells were
758 lysed and RNA was purified using an RNeasy purification kit (Qiagen). RNA quality was assessed using
759 an Agilent 2100 Bioanalyzer, and all samples had RIN values above 8.0. Transcripts were selected
760 using polyA selection (using Dynabeads mRNA Purification Kit, Invitrogen) and enzymatically
761 fragmented as part of the Apollo library prep kits (Wafergen PrepX RNA library prep for Illumina).
762 Libraries were constructed by using Apollo 324 (IntegenX Inc.), PCR-amplified, and multiplexed at the
763 Functional Genomics Lab at the University of California, Berkeley (<http://qb3.berkeley.edu/qb3/fgl/>). The
764 resulting libraries were sequenced at the Vincent J. Coates Genomics Sequencing Facility at the
765 University of California, Berkeley using single-end reads, 50 base length, with the Hiseq 2000 Illumina
766 platform. Sequence data were aligned to the *Mus musculus* C57BL/6 reference genome (reference
767 assembly GCA_000001635.8) using CLC Genomics Workbench (Qiagen). Fold regulation of genes for
768 each genotype was determined by referencing the sample uninfected, untreated BMDMs. Comparisons
769 were then made between the sequencing results from the infected, IFN-I-treated WT and the *Irf* mutant
770 genes. Each data set was composed of at least 55 million reads and 98.3% of the reads aligned with
771 the reference. Genes with low abundance of reads (Reads Per Kilobase of transcript, per Million
772 mapped reads, RPKM, of <10) in the infected WT BMDMs treated with IFN-I were excluded from the
773 analysis. Sequencing data were uploaded to GEO, accession number GSE128211.

774

775 **Microscopy**

776 For brightfield microscopy, images were captured using an IX71 Olympus microscope with a
777 UCPLFLN 20x 0.7 NA objective, OptiMOS sCMOS camera (QImaging), and Micro-Manager software
778 (Edelstein et al., 2014). For immunofluorescence microscopy, 2.5-5 x 10⁵ BMDMs were plated overnight
779 in BMDM media in 24-well plates with sterile 12 mm coverslips (Thermo Fisher Scientific, 12-545-80).
780 Infections were performed as described above. At the indicated times post-infection, coverslips were
781 washed once with PBS and fixed in 4% paraformaldehyde (Ted Pella Inc., 18505, diluted in 1 x PBS)

782 for 10 min at room temperature. Coverslips were then washed 3 times in PBS. Coverslips were washed
783 once in blocking buffer (1 x PBS with 2% BSA) and permeabilized with 0.5% triton X-100 for 10 min.
784 Coverslips were incubated with primary and secondary antibodies diluted in 2% BSA in PBS, each for
785 30 min at room temperature. *R. parkeri* were detected using mouse anti-*Rickettsia* 14-13 (originally
786 from Dr. Ted Hackstadt, NIH/NIAID Rocky Mountain Laboratories). GBP2 was detected with anti-GBP2
787 (ProteinTech, 11854-1-AP; Research Resource Identifier AB_2109336). Nuclei were stained with DAPI,
788 and actin was stained with Alexa-568 phalloidin (Life Technologies, A12380). Secondary antibodies
789 were Alexa-405 goat anti-mouse (A31553) and Alexa-488 goat anti-rabbit (A11008). Coverslips were
790 mounted in Prolong mounting media (Invitrogen). Samples were imaged with the Nikon Ti Eclipse
791 microscope with a Yokogawa CSU-X1 spinning disc confocal with 60X and 100X (1.4 NA) Plan Apo
792 objectives, and a Clara Interline CCD Camera (Andor Technology) using MetaMorph software
793 (Molecular Devices). Rendered Z-stacks were used for quantifications. Images were processed using
794 FIJI (Schindelin et al., 2012) and brightness and contrast adjustments were applied to entire images.
795 Images were assembled using Adobe Illustrator. Representative images are a single optical section, in
796 which most or all bacteria were in the focal plane.

797

798 ***In vitro* assays**

799 For LDH assays, 60 μ l of supernatant from wells containing BMDMs was collected into 96-well
800 plates. 60 μ l of LDH buffer was then added. LDH buffer contained: 3 μ l of "INT" solution containing 2
801 mg/ml tetrazolium salt (Sigma I8377) in PBS; 3 μ l of "DIA" solution containing 13.5 units/ml diaphorase
802 (Sigma, D5540), 3 mg/ml β -nicotinamide adenine dinucleotide hydrate (Sigma, N3014), 0.03% BSA,
803 and 1.2% sucrose; 34 μ l PBS with 0.5% BSA; and 20 μ l solution containing 36 mg/ml lithium lactate in
804 10 mM Tris HCl pH 8.5 (Sigma L2250). Supernatant from uninfected cells and from cells completely
805 lysed with 1% triton X-100 (final concentration) were used as controls. Reactions were incubated at
806 room temperature for 20 min prior to reading at 490 nm absorbance using an Infinite F200 Pro plate
807 reader (Tecan). Values for uninfected cells were subtracted from the experimental values, divided by

808 the difference of triton-lysed and uninfected cells, and multiplied by 100 to obtain percent lysis. Each
809 experiment was performed and averaged between technical duplicates and biological duplicates.

810 For the IFN-I bioassay experiments, 5×10^4 3T3 cells containing an interferon-sensitive
811 response element (ISRE) fused to luciferase (Jiang et al., 2005; McWhirter et al., 2009) were plated per
812 well into 96-well white-bottom plates (Greiner 655083) in DMEM containing 10% FBS, 100 U/ml
813 penicillin and 100 µg/ml streptomycin. 24 h later, media was replaced and confluent cells were treated
814 with 2 µl of supernatant harvested from BMDM experiments. After 4 h, media was removed and cells
815 were lysed with 40 µl TNT lysis buffer (20 mM Tris, pH 8, 200 mM NaCl, 1% triton-100). Lysates were
816 then injected with 40 µl firefly luciferin substrate (Biosynth) and luminescence was measured using a
817 SpectraMax L plate reader (Molecular Devices).

818

819 **qPCR**

820 For qPCR experiments using mouse tissue, 50 µl of organ homogenates was added to 600 µl
821 of RLT buffer (Qiagen) containing 1% β-mercaptoethanol and frozen at -80°C. Frozen lysates were later
822 thawed and RNA was purified and treated with DNase, according to the manufacturer's protocol using
823 an RNeasy kit (Qiagen). RNA abundance was quantified using a NanoDrop ND-1000 and 200 ng RNA
824 was *in vitro* transcribed (ProtoScript II, NEB, M0368S) and diluted 10x in sterile nuclease-free water.
825 Real-time PCR was performed using SYBR Green (Thermo, A25742), 2 µl of cDNA, and 1 µM each of
826 the following oligonucleotides: actin F: GGCTGTATTCCCCTCCATCG; actin R:
827 GTCACCCACATAGGAGTCCTTC; IFN-β F: AGCTCCAAGAAAGGACGAACAT; and IFN-β R:
828 CCCTGTAGGTGAGGTTGATCTT. For normalization, values for IFN-β were divided by values for actin.
829 Measurements were acquired with a QuantStudio 5 real-time qPCR machine (Applied Biosystems).

830

831 **QUANTIFICATION AND STATISTICAL ANALYSIS**

832 Statistical parameters and significance are reported in the figures and the figure legends. Data
833 are determined to be statistically significant when $p < 0.05$ by an unpaired two-tailed Student's T-Test an
834 ANOVA with multiple comparisons post-hoc test. For *in vivo* PFU data, data are determined to be

835 statistically significant when $p < 0.05$ by a Mann-Whitney U test. Asterisks denote statistical significance
836 as: *, $p < 0.05$; **, $p < 0.01$; ***, $p < 0.001$; ****, $p < 0.0001$, compared to indicated controls. For animal
837 experiments, bars denote medians. Error bars indicate standard error (SE). All other graphical
838 representations are described in the figure legends. Statistical analyses were performed using
839 GraphPad PRISM.

840

841

842 **Table S1. Related to Figure 3. RNA-seq analysis of genes regulated by IRFs during *R. parkeri***
843 **infection and IFN-I treatment.**

844

845

846

847 **References**

848 Aachoui, Y., Leaf, I.A., Hagar, J.A., Fontana, M.F., Campos, C.G., Zak, D.E., Tan, M.H., Cotter, P.A.,
849 Vance, R.E., Aderem, A., et al. (2013). Caspase-11 protects against bacteria that escape the vacuole.
850 *Science* 339, 975–978.

851 Auerbuch, V., Brockstedt, D.G., Meyer-Morse, N., O’Riordan, M., and Portnoy, D.A. (2004). Mice
852 lacking the type I interferon receptor are resistant to *Listeria monocytogenes*. *The Journal of*
853 *Experimental Medicine* 200, 527–533.

854 Banajee, K.H., Embers, M.E., Langohr, I.M., Doyle, L.A., Hasenkampf, N.R., and Macaluso, K.R.
855 (2015). *Amblyomma maculatum* Feeding Augments *Rickettsia parkeri* Infection in a Rhesus Macaque
856 Model: A Pilot Study. *PLoS ONE* 10, e0135175.

857 Banerjee, I., Behl, B., Mendonca, M., Shrivastava, G., Russo, A.J., Menoret, A., Ghosh, A., Vella,
858 A.T., Vanaja, S.K., Sarkar, S.N., et al. (2018). Gasdermin D Restrains Type I Interferon Response to
859 Cytosolic DNA by Disrupting Ionic Homeostasis. *Immunity* 49, 413–426.e415.

860 Bauler, T.J., Chase, J.C., and Bosio, C.M. (2011). IFN- β mediates suppression of IL-12p40 in human
861 dendritic cells following infection with virulent *Francisella tularensis*. *J. Immunol.* 187, 1845–1855.

862 Boxx, G.M., and Cheng, G. (2016). The Roles of Type I Interferon in Bacterial Infection. *Cell Host*
863 *Microbe* 19, 760–769.

864 Brubaker, S.W., Bonham, K.S., Zanoni, I., and Kagan, J.C. (2015). Innate immune pattern recognition:
865 a cell biological perspective. *Annual Review of Immunology* 33, 257–290.

866 Burdette, D.L., Monroe, K.M., Sotelo-Troha, K., Iwig, J.S., Eckert, B., Hyodo, M., Hayakawa, Y., and
867 Vance, R.E. (2011). STING is a direct innate immune sensor of cyclic di-GMP. *Nature* 478, 515–518.

868 Carlin, A.F., Plummer, E.M., Vizcarra, E.A., Sheets, N., Joo, Y., Tang, W., Day, J., Greenbaum, J.,

- 869 Glass, C.K., Diamond, M.S., et al. (2017). An IRF-3-, IRF-5-, and IRF-7-Independent Pathway of
870 *Dengue* Viral Resistance Utilizes IRF-1 to Stimulate Type I and II Interferon Responses. *Cell Rep* 21,
871 1600–1612.
- 872 Carrero, J.A. (2013). Confounding roles for type I interferons during bacterial and viral pathogenesis.
873 *Int. Immunol.* 25, 663–669.
- 874 Colonne, P.M., Eremeeva, M.E., and Sahni, S.K. (2011). Beta interferon-mediated activation of signal
875 transducer and activator of transcription protein 1 interferes with *Rickettsia conorii* replication in
876 human endothelial cells. *Infect. Immun.* 79, 3733–3743.
- 877 Colonne, P.M., Sahni, A., and Sahni, S.K. (2013). Suppressor of cytokine signalling protein SOCS1
878 and UBP43 regulate the expression of type I interferon-stimulated genes in human microvascular
879 endothelial cells infected with *Rickettsia conorii*. *J. Med. Microbiol.* 62, 968–979.
- 880 Corrales, L., Woo, S.-R., Williams, J.B., McWhirter, S.M., Dubensky, T.W., and Gajewski, T.F. (2016).
881 Antagonism of the STING Pathway via Activation of the AIM2 Inflammasome by Intracellular DNA. *J.*
882 *Immunol.* 196, 3191–3198.
- 883 Edelstein, A.D., Tsuchida, M.A., Amodaj, N., Pinkard, H., Vale, R.D., and Stuurman, N. (2014).
884 Advanced methods of microscope control using µManager software. *J Biol Methods* 1, 10.
- 885 Feng, H.M., and Walker, D.H. (1993). Interferon-gamma and tumor necrosis factor-alpha exert their
886 antirickettsial effect via induction of synthesis of nitric oxide. *Am. J. Pathol.* 143, 1016–1023.
- 887 Feng, H.M., and Walker, D.H. (2000). Mechanisms of intracellular killing of *Rickettsia conorii* in
888 infected human endothelial cells, hepatocytes, and macrophages. *Infect. Immun.* 68, 6729–6736.
- 889 Feng, H.M., Popov, V.L., and Walker, D.H. (1994). Depletion of gamma interferon and tumor necrosis
890 factor alpha in mice with *Rickettsia conorii*-infected endothelium: impairment of rickettsicidal nitric
891 oxide production resulting in fatal, overwhelming rickettsial disease. *Infect. Immun.* 62, 1952–1960.
- 892 Feng, H.M., Wen, J., and Walker, D.H. (1993). *Rickettsia australis* infection: a murine model of a
893 highly invasive vasculopathic rickettsiosis. *Am. J. Pathol.* 142, 1471–1482.
- 894 Fensterl, V., Wetzel, J.L., Ramachandran, S., Ogino, T., Stohlman, S.A., Bergmann, C.C., Diamond,
895 M.S., Virgin, H.W., and Sen, G.C. (2012). Interferon-induced *Iffit2/ISG54* protects mice from lethal VSV
896 neuropathogenesis. *PLoS Pathog.* 8, e1002712.
- 897 Guarda, G., Braun, M., Staehli, F., Tardivel, A., Mattmann, C., Förster, I., Farlik, M., Decker, T.,
898 Pasquier, Du, R.A., Romero, P., et al. (2011). Type I interferon inhibits interleukin-1 production and
899 inflammasome activation. *Immunity* 34, 213–223.
- 900 Hagar, J.A., Powell, D.A., Aachoui, Y., Ernst, R.K., and Miao, E.A. (2013). Cytoplasmic LPS activates
901 caspase-11: implications in TLR4-independent endotoxic shock. *Science* 341, 1250–1253.
- 902 Henry, T., Kirimanjeswara, G.S., Ruby, T., Jones, J.W., Peng, K., Perret, M., Ho, L., Sauer, J.-D.,
903 Iwakura, Y., Metzger, D.W., et al. (2010). Type I IFN signaling constrains IL-17A/F secretion by
904 gamma delta T cells during bacterial infections. *J. Immunol.* 184, 3755–3767.
- 905 Hernandez-Cuellar, E., Tsuchiya, K., Hara, H., Fang, R., Sakai, S., Kawamura, I., Akira, S., and
906 Mitsuyama, M. (2012). Cutting edge: nitric oxide inhibits the NLRP3 inflammasome. *J. Immunol.* 189,
907 5113–5117.

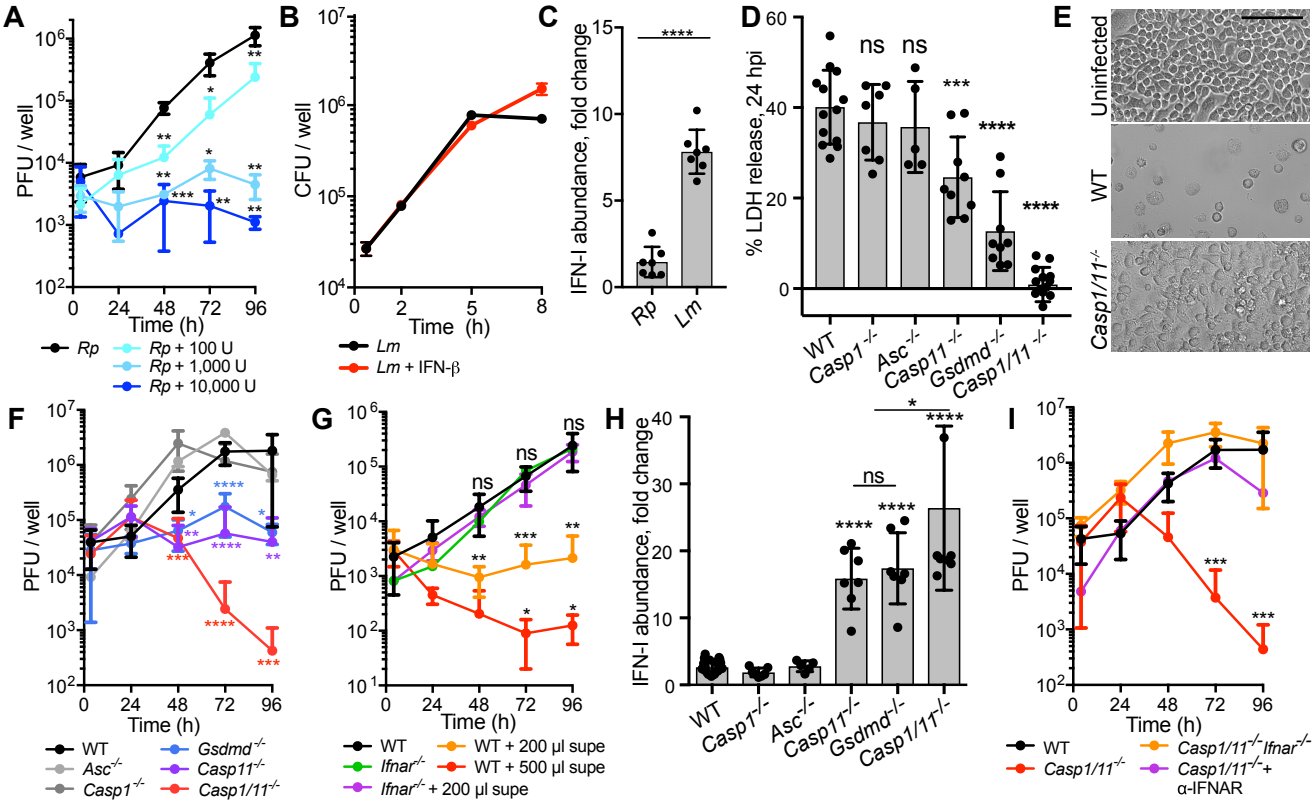
- 908 Huang, S., Hendriks, W., Althage, A., Hemmi, S., Bluethmann, H., Kamijo, R., Vilcek, J., Zinkernagel,
909 R.M., and Aguet, M. (1993). Immune response in mice that lack the interferon-gamma receptor.
910 *Science* 259, 1742–1745.
- 911 Inoue, M., Williams, K.L., Oliver, T., Vandenabeele, P., Rajan, J.V., Miao, E.A., and Shinohara, M.L.
912 (2012). Interferon- β therapy against EAE is effective only when development of the disease depends
913 on the NLRP3 inflammasome. *Sci Signal* 5, ra38–ra38.
- 914 Ishida, T., Choi, S., Kundu, R.K., Hirata, K.-I., Rubin, E.M., Cooper, A.D., and Quertermous, T. (2003).
915 Endothelial lipase is a major determinant of HDL level. *J. Clin. Invest.* 111, 347–355.
- 916 Jabir, M.S., Ritchie, N.D., Li, D., Bayes, H.K., Tourlomousis, P., Puleston, D., Lupton, A., Hopkins, L.,
917 Simon, A.K., Bryant, C., et al. (2014). Caspase-1 cleavage of the TLR adaptor TRIF inhibits
918 autophagy and β -interferon production during *Pseudomonas aeruginosa* infection. *Cell Host Microbe*
919 15, 214–227.
- 920 Jiang, Z., Georgel, P., Du, X., Shamel, L., Sovath, S., Mudd, S., Huber, M., Kalis, C., Keck, S.,
921 Galanos, C., et al. (2005). CD14 is required for MyD88-independent LPS signaling. *Nat. Immunol.* 6,
922 565–570.
- 923 Jorgensen, I., and Miao, E.A. (2015). Pyroptotic cell death defends against intracellular pathogens.
924 *Immunological Reviews* 265, 130–142.
- 925 Kayagaki, N., Stowe, I.B., Lee, B.L., O'Rourke, K., Anderson, K., Warming, S., Cuellar, T., Haley, B.,
926 Roose-Girma, M., Phung, Q.T., et al. (2015). Caspase-11 cleaves gasdermin D for non-canonical
927 inflammasome signalling. *Nature* 526, 666–671.
- 928 Kayagaki, N., Wong, M.T., Stowe, I.B., Ramani, S.R., Gonzalez, L.C., Akashi-Takamura, S., Miyake,
929 K., Zhang, J., Lee, W.P., Muszyński, A., et al. (2013). Noncanonical inflammasome activation by
930 intracellular LPS independent of TLR4. *Science* 341, 1246–1249.
- 931 Lamkanfi, M., and Dixit, V.M. (2014). Mechanisms and functions of inflammasomes. *Cell* 157, 1013–
932 1022.
- 933 Li, H., Jerrells, T.R., Spitalny, G.L., and Walker, D.H. (1987). Gamma interferon as a crucial host
934 defense against *Rickettsia conorii* in vivo. *Infect. Immun.* 55, 1252–1255.
- 935 Liu, B.C., Sarhan, J., Panda, A., Muendlein, H.I., Ilyukha, V., Coers, J., Yamamoto, M., Isberg, R.R.,
936 and Poltorak, A. (2018). Constitutive Interferon Maintains GBP Expression Required for Release of
937 Bacterial Components Upstream of Pyroptosis and Anti-DNA Responses. *Cell Rep* 24, 155–
938 168.e155.
- 939 MacMicking, J.D. (2012). Interferon-inducible effector mechanisms in cell-autonomous immunity. *Nat.*
940 *Rev. Immunol.* 12, 367–382.
- 941 Maltez, V.I., Tubbs, A.L., Cook, K.D., Aachoui, Y., Falcone, E.L., Holland, S.M., Whitmire, J.K., and
942 Miao, E.A. (2015). Inflammasomes Coordinate Pyroptosis and Natural Killer Cell Cytotoxicity to Clear
943 Infection by a Ubiquitous Environmental Bacterium. *Immunity* 43, 987–997.
- 944 Marcus, A., Mao, A.J., Lensink-Vasan, M., Wang, L., Vance, R.E., and Raulet, D.H. (2018). Tumor-
945 Derived cGAMP Triggers a STING-Mediated Interferon Response in Non-tumor Cells to Activate the
946 NK Cell Response. *Immunity* 49, 754–763.e754.
- 947 Matsuyama, T., Kimura, T., Kitagawa, M., Pfeffer, K., Kawakami, T., Watanabe, N., Kundig, T.M.,

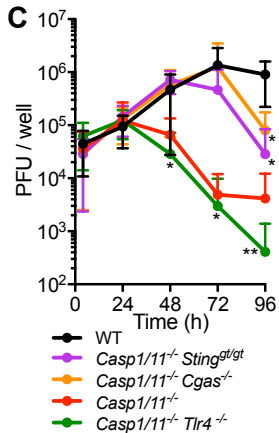
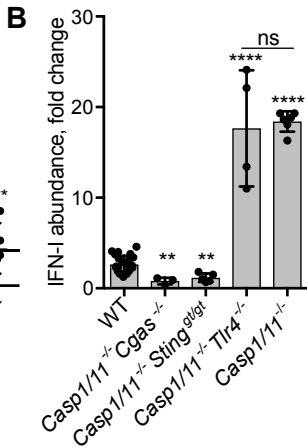
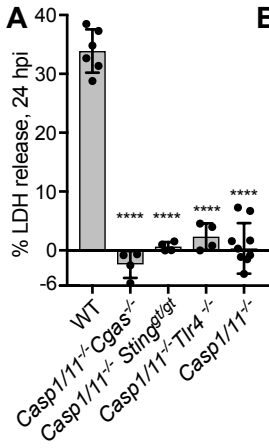
- 948 Amakawa, R., Kishihara, K., and Wakeham, A. (1993). Targeted disruption of IRF-1 or IRF-2 results in
949 abnormal type I IFN gene induction and aberrant lymphocyte development. *Cell* 75, 83–97.
- 950 McNab, F., Mayer-Barber, K., Sher, A., Wack, A., and O'Garra, A. (2015). Type I interferons in
951 infectious disease. *Nat. Rev. Immunol.* 15, 87–103.
- 952 McWhirter, S.M., Barbalat, R., Monroe, K.M., Fontana, M.F., Hyodo, M., Joncker, N.T., Ishii, K.J.,
953 Akira, S., Colonna, M., Chen, Z.J., et al. (2009). A host type I interferon response is induced by
954 cytosolic sensing of the bacterial second messenger cyclic-di-GMP. *The Journal of Experimental*
955 *Medicine* 206, 1899–1911.
- 956 Meunier, E., and Broz, P. (2016). Interferon-inducible GTPases in cell autonomous and innate
957 immunity. *Cell. Microbiol.* 18, 168–180.
- 958 Miao, E.A., Leaf, I.A., Treuting, P.M., Mao, D.P., Dors, M., Sarkar, A., Warren, S.E., Wewers, M.D.,
959 and Aderem, A. (2010). Caspase-1-induced pyroptosis is an innate immune effector mechanism
960 against intracellular bacteria. *Nat. Immunol.* 11, 1136–1142.
- 961 Milligan, G.N., Sarathy, V.V., White, M.M., Greenberg, M.B., Campbell, G.A., Pyles, R.B., Barrett,
962 A.D.T., and Bourne, N. (2017). A lethal model of disseminated *dengue virus* type 1 infection in AG129
963 mice. *J. Gen. Virol.* 98, 2507–2519.
- 964 Mishra, B.B., Rathinam, V.A.K., Martens, G.W., Martinot, A.J., Kornfeld, H., Fitzgerald, K.A., and
965 Sasseti, C.M. (2013). Nitric oxide controls the immunopathology of tuberculosis by inhibiting NLRP3
966 inflammasome-dependent processing of IL-1 β . *Nat. Immunol.* 14, 52–60.
- 967 Mitchell, G., and Isberg, R.R. (2017). Innate Immunity to Intracellular Pathogens: Balancing Microbial
968 Elimination and Inflammation. *Cell Host Microbe* 22, 166–175.
- 969 Müller, U., Steinhoff, U., Reis, L.F., Hemmi, S., Pavlovic, J., Zinkernagel, R.M., and Aguet, M. (1994).
970 Functional role of type I and type II interferons in antiviral defense. *Science* 264, 1918–1921.
- 971 O'Connell, R.M., Saha, S.K., Vaidya, S.A., Bruhn, K.W., Miranda, G.A., Zarnegar, B., Perry, A.K.,
972 Nguyen, B.O., Lane, T.F., Taniguchi, T., et al. (2004). Type I interferon production enhances
973 susceptibility to *Listeria monocytogenes* infection. *The Journal of Experimental Medicine* 200, 437–
974 445.
- 975 Osterloh, A., Papp, S., Moderzynski, K., Kuehl, S., Richardt, U., and Fleischer, B. (2016). Persisting
976 *Rickettsia typhi* Causes Fatal Central Nervous System Inflammation. *Infect. Immun.* 84, 1615–1632.
- 977 Papp, S., Moderzynski, K., Rauch, J., Heine, L., Kuehl, S., Richardt, U., Mueller, H., Fleischer, B., and
978 Osterloh, A. (2016). Liver Necrosis and Lethal Systemic Inflammation in a Murine Model of *Rickettsia*
979 *typhi* Infection: Role of Neutrophils, Macrophages and NK Cells. *PLoS Negl Trop Dis* 10, e0004935.
- 980 Peng, K., Broz, P., Jones, J., Joubert, L.-M., and Monack, D. (2011). Elevated AIM2-mediated
981 pyroptosis triggered by hypercytotoxic Francisella mutant strains is attributed to increased intracellular
982 bacteriolysis. *Cell. Microbiol.* 13, 1586–1600.
- 983 Pilla-Moffett, D., Barber, M.F., Taylor, G.A., and Coers, J. (2016). Interferon-Inducible GTPases in
984 Host Resistance, Inflammation and Disease. *J. Mol. Biol.* 428, 3495–3513.
- 985 Proenca-Modena, J.L., Hyde, J.L., Sesti-Costa, R., Lucas, T., Pinto, A.K., Richner, J.M., Gorman,
986 M.J., Lazear, H.M., and Diamond, M.S. (2016). Interferon-Regulatory Factor 5-Dependent Signaling
987 Restricts *Orthobunyavirus* Dissemination to the Central Nervous System. *J. Virol.* 90, 189–205.

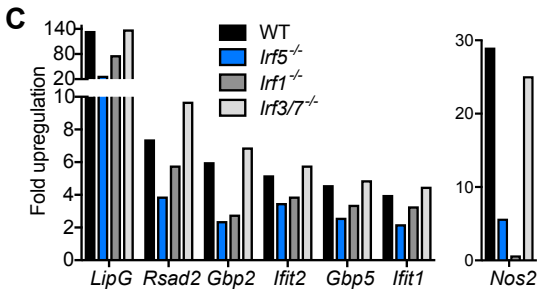
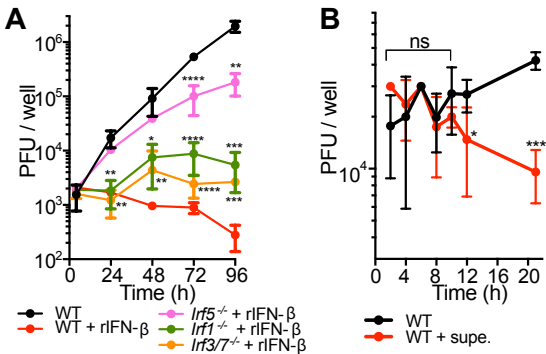
- 988 Purtha, W.E., Swiecki, M., Colonna, M., Diamond, M.S., and Bhattacharya, D. (2012). Spontaneous
989 mutation of the *Dock2* gene in *Irf5*^{-/-} mice complicates interpretation of type I interferon production
990 and antibody responses. *Proc. Natl. Acad. Sci. U.S.a.* 109, E898–E904.
- 991 Randow, F., MacMicking, J.D., and James, L.C. (2013). Cellular self-defense: how cell-autonomous
992 immunity protects against pathogens. *Science* 340, 701–706.
- 993 Rauch, I., Deets, K.A., Ji, D.X., Moltke, von, J., Tenthorey, J.L., Lee, A.Y., Philip, N.H., Ayres, J.S.,
994 Brodsky, I.E., Gronert, K., et al. (2017). NAIP-NLRC4 Inflammasomes Coordinate Intestinal Epithelial
995 Cell Expulsion with Eicosanoid and IL-18 Release via Activation of Caspase-1 and -8. *Immunity* 46,
996 649–659.
- 997 Rayamajhi, M., Humann, J., Penheiter, K., Andreasen, K., and Lenz, L.L. (2010). Induction of IFN-
998 alphabeta enables *Listeria monocytogenes* to suppress macrophage activation by IFN-gamma. *The*
999 *Journal of Experimental Medicine* 207, 327–337.
- 1000 Reutterer, B., Stockinger, S., Pilz, A., Soulat, D., Kastner, R., Westermayer, S., Rüllicke, T., Müller, M.,
1001 and Decker, T. (2008). Type I IFN are host modulators of strain-specific *Listeria monocytogenes*
1002 virulence. *Cell. Microbiol.* 10, 1116–1129.
- 1003 Rossi, S.L., Tesh, R.B., Azar, S.R., Muruato, A.E., Hanley, K.A., Auguste, A.J., Langsjoen, R.M.,
1004 Paessler, S., Vasilakis, N., and Weaver, S.C. (2016). Characterization of a Novel Murine Model to
1005 Study *Zika Virus*. *Am. J. Trop. Med. Hyg.* 94, 1362–1369.
- 1006 Sahni, S.K., and Rydkina, E. (2009). Host-cell interactions with pathogenic *Rickettsia* species. *Future*
1007 *Microbiol* 4, 323–339.
- 1008 Sauer, J.-D., Sotelo-Troha, K., Moltke, von, J., Monroe, K.M., Rae, C.S., Brubaker, S.W., Hyodo, M.,
1009 Hayakawa, Y., Woodward, J.J., Portnoy, D.A., et al. (2011). The N-ethyl-N-nitrosourea-induced
1010 Goldenticket mouse mutant reveals an essential function of *Sting* in the in vivo interferon response to
1011 *Listeria monocytogenes* and cyclic dinucleotides. *Infect. Immun.* 79, 688–694.
- 1012 Sauer, J.-D., Witte, C.E., Zemansky, J., Hanson, B., Lauer, P., and Portnoy, D.A. (2010). *Listeria*
1013 *monocytogenes* triggers AIM2-mediated pyroptosis upon infrequent bacteriolysis in the macrophage
1014 cytosol. *Cell Host Microbe* 7, 412–419.
- 1015 Schindelin, J., Arganda-Carreras, I., Frise, E., Kaynig, V., Longair, M., Pietzsch, T., Preibisch, S.,
1016 Rueden, C., Saalfeld, S., Schmid, B., et al. (2012). Fiji: an open-source platform for biological-image
1017 analysis. *Nat. Methods* 9, 676–682.
- 1018 Shen, A., and Higgins, D.E. (2006). The MogR transcriptional repressor regulates nonhierarchal
1019 expression of flagellar motility genes and virulence in *Listeria monocytogenes*. *PLoS Pathog.* 2, e30.
- 1020 Shi, J., Zhao, Y., Wang, K., Shi, X., Wang, Y., Huang, H., Zhuang, Y., Cai, T., Wang, F., and Shao, F.
1021 (2015). Cleavage of GSDMD by inflammatory caspases determines pyroptotic cell death. *Nature* 526,
1022 660–665.
- 1023 Shi, J., Zhao, Y., Wang, Y., Gao, W., Ding, J., Li, P., Hu, L., and Shao, F. (2014). Inflammatory
1024 caspases are innate immune receptors for intracellular LPS. *Nature* 514, 187–192.
- 1025 Smalley, C., Bechelli, J., Rockx-Brouwer, D., Saito, T., Azar, S.R., Ismail, N., Walker, D.H., and Fang,
1026 R. (2016). *Rickettsia australis* Activates Inflammasome in Human and Murine Macrophages. *PLoS*
1027 *ONE* 11, e0157231.

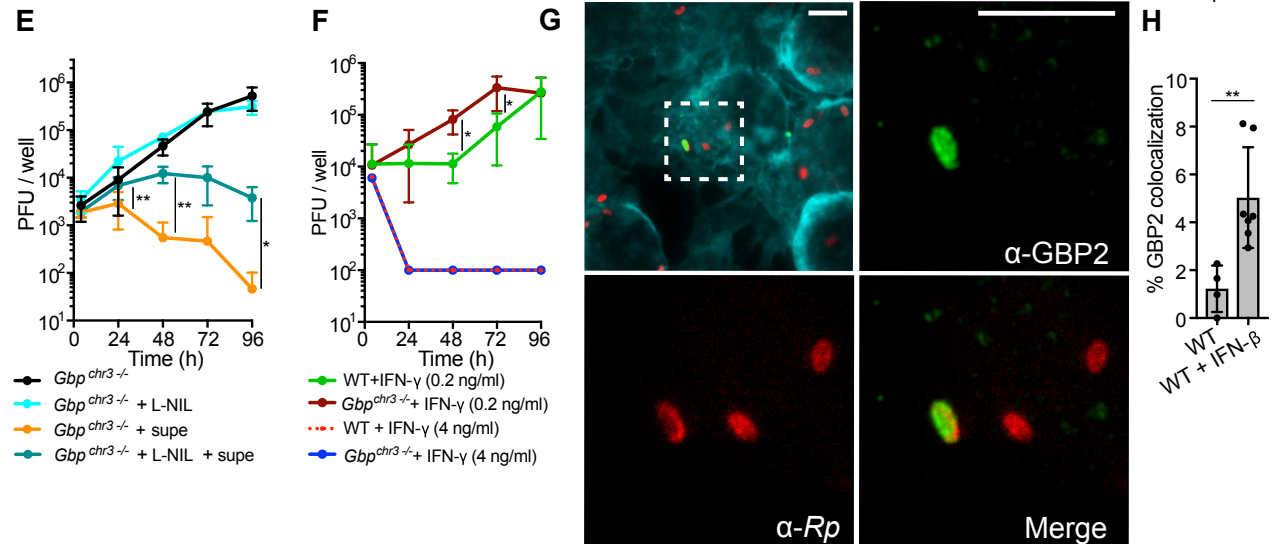
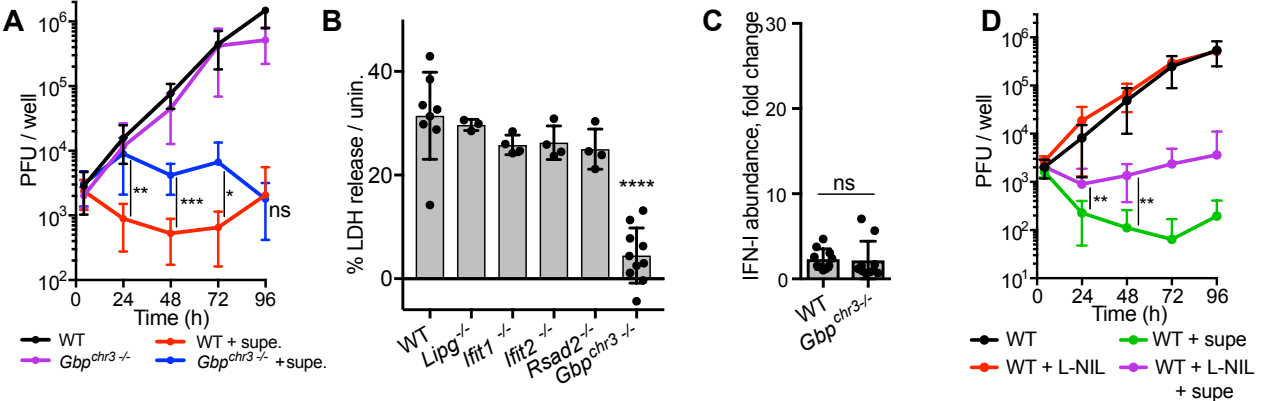
- 1028 Stetson, D.B., and Medzhitov, R. (2006). Type I interferons in host defense. *Immunity* 25, 373–381.
- 1029 Storek, K.M., Gertszov, N.A., Ohlson, M.B., and Monack, D.M. (2015). cGAS and Ifi204 cooperate to
1030 produce type I IFNs in response to *Francisella* infection. *J. Immunol.* 194, 3236–3245.
- 1031 Strowig, T., Henao-Mejia, J., Elinav, E., and Flavell, R. (2012). Inflammasomes in health and disease.
1032 *Nature* 481, 278–286.
- 1033 Sun, L., Wu, J., Du, F., Chen, X., and Chen, Z.J. (2013). Cyclic GMP-AMP synthase is a cytosolic
1034 DNA sensor that activates the type I interferon pathway. *Science* 339, 786–791.
- 1035 Szretter, K.J., Daniels, B.P., Cho, H., Gainey, M.D., Yokoyama, W.M., Gale, M., Virgin, H.W., Klein,
1036 R.S., Sen, G.C., and Diamond, M.S. (2012). 2'-O methylation of the viral mRNA cap by *West Nile*
1037 *virus* evades *ifit1*-dependent and -independent mechanisms of host restriction in vivo. *PLoS Pathog.*
1038 8, e1002698.
- 1039 Takeuchi, O., and Akira, S. (2010). Pattern recognition receptors and inflammation. *Cell* 140, 805–
1040 820.
- 1041 Thackray, L.B., Shrestha, B., Richner, J.M., Miner, J.J., Pinto, A.K., Lazear, H.M., Gale, M., and
1042 Diamond, M.S. (2014). Interferon regulatory factor 5-dependent immune responses in the draining
1043 lymph node protect against *West Nile virus* infection. *J. Virol.* 88, 11007–11021.
- 1044 Turco, J., and Winkler, H.H. (1990). Interferon-alpha/beta and *Rickettsia prowazekii*: induction and
1045 sensitivity. *Ann. N. Y. Acad. Sci.* 590, 168–186.
- 1046 Turco, J., and Winkler, H.H. (1993). Role of the nitric oxide synthase pathway in inhibition of growth of
1047 interferon-sensitive and interferon-resistant *Rickettsia prowazekii* strains in L929 cells treated with
1048 tumor necrosis factor alpha and gamma interferon. *Infect. Immun.* 61, 4317–4325.
- 1049 Turco, J., Liu, H., Gottlieb, S.F., and Winkler, H.H. (1998). Nitric oxide-mediated inhibition of the ability
1050 of *Rickettsia prowazekii* to infect mouse fibroblasts and mouse macrophagelike cells. *Infect. Immun.*
1051 66, 558–566.
- 1052 Ulland, T.K., Buchan, B.W., Ketterer, M.R., Fernandes-Alnemri, T., Meyerholz, D.K., Apicella, M.A.,
1053 Alnemri, E.S., Jones, B.D., Nauseef, W.M., and Sutterwala, F.S. (2010). Cutting edge: mutation of
1054 *Francisella tularensis mviN* leads to increased macrophage *absent in melanoma 2* inflammasome
1055 activation and a loss of virulence. *J. Immunol.* 185, 2670–2674.
- 1056 Walker, D.H., Hudnall, S.D., Szaniawski, W.K., and Feng, H.M. (1999). Monoclonal antibody-based
1057 immunohistochemical diagnosis of rickettsialpox: the macrophage is the principal target. *Mod. Pathol.*
1058 12, 529–533.
- 1059 Walker, D.H., Popov, V.L., Crocquet-Valdes, P.A., Welsh, C.J., and Feng, H.M. (1997). Cytokine-
1060 induced, nitric oxide-dependent, intracellular antirickettsial activity of mouse endothelial cells. *Lab.*
1061 *Invest.* 76, 129–138.
- 1062 Walker, D.H., and Ismail, N. (2008). Emerging and re-emerging rickettsioses: endothelial cell infection
1063 and early disease events. *Nat. Rev. Microbiol.* 6, 375–386.
- 1064 Wallet, P., Lagrange, B., and Henry, T. (2016). *Francisella* Inflammasomes: Integrated Responses to
1065 a Cytosolic Stealth Bacterium. In *Inflammasome Signaling and Bacterial Infections*, (Cham: Springer
1066 International Publishing), pp. 229–256.

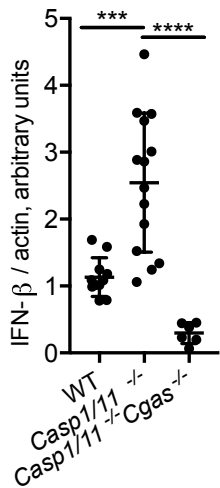
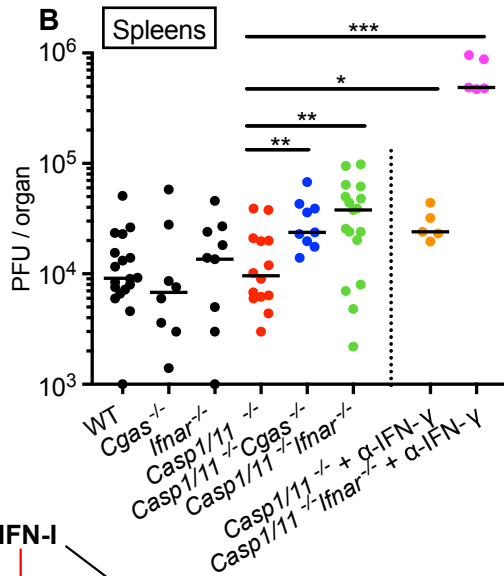
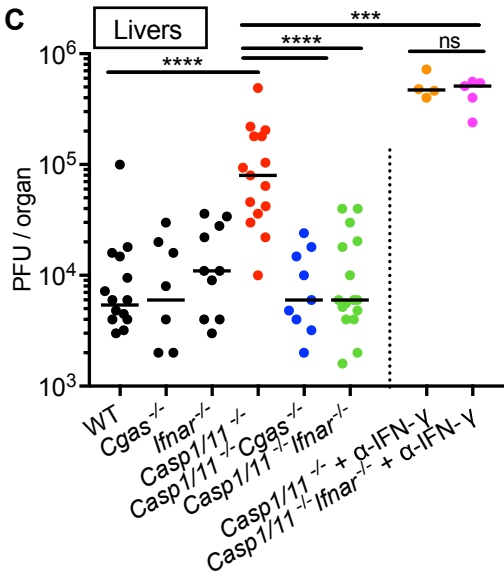
- 1067 Wang, S., Miura, M., Jung, Y.K., Zhu, H., Li, E., and Yuan, J. (1998). Murine caspase-11, an ICE-
1068 interacting protease, is essential for the activation of ICE. *Cell* 92, 501–509.
- 1069 Wang, Y., Ning, X., Gao, P., Wu, S., Sha, M., Lv, M., Zhou, X., Gao, J., Fang, R., Meng, G., et al.
1070 (2017). Inflammasome Activation Triggers Caspase-1-Mediated Cleavage of cGAS to Regulate
1071 Responses to DNA Virus Infection. *Immunity* 46, 393–404.
- 1072 Weiss, G., and Schaible, U.E. (2015). Macrophage defense mechanisms against intracellular
1073 bacteria. *Immunological Reviews* 264, 182–203.
- 1074 Woods, M.E., Wen, G., and Olano, J.P. (2005). Nitric oxide as a mediator of increased microvascular
1075 permeability during acute rickettsioses. *Ann. N. Y. Acad. Sci.* 1063, 239–245.
- 1076 Woodward, J.J., Iavarone, A.T., and Portnoy, D.A. (2010). c-di-AMP secreted by intracellular *Listeria*
1077 *monocytogenes* activates a host type I interferon response. *Science* 328, 1703–1705.
- 1078 Yamamoto, M., Okuyama, M., Ma, J.S., Kimura, T., Kamiyama, N., Saiga, H., Ohshima, J., Sasai, M.,
1079 Kayama, H., Okamoto, T., et al. (2012). A cluster of interferon- γ -inducible p65 GTPases plays a
1080 critical role in host defense against *Toxoplasma gondii*. *Immunity* 37, 302–313.
- 1081









A**B****C****D**